

AD-A063 326

DOUGLAS AIRCRAFT CO LONG BEACH CALIF
A GENERAL METHOD FOR CALCULATING THREE-DIMENSIONAL LAMINAR AND --ETC(U)
OCT 78 T CEBECI, K C CHANG, K KAUPS

F/G 20/4
N00014-76-C-0950
NL

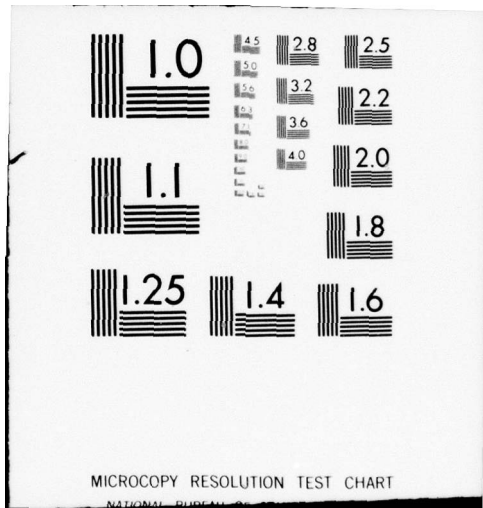
UNCLASSIFIED

MDC-J7998

| OF |
AD
A063 326



END
DATE
FILMED
3-79
DDC



MICROCOPY RESOLUTION TEST CHART

NATIONAL BUREAU OF STANDARDS-1963-A

LEVEL

REPORT NO. NDC J7908

12

9

A GENERAL METHOD FOR CALCULATING THREE-DIMENSIONAL LAMINAR AND TURBULENT BOUNDARY LAYERS ON SHIP HULLS

by

Tuncer Cabot, K. G. Chang and Kale Kaups

October 1978

Jan 14 1979

AD A0 633 26

This research was carried out under the Naval Sea
Systems Command General Hydromechanics Research
Program subproject SR 023 01 01, administered by the
W. Taylor Naval Ship Research and Development Center
under contract N00014-76-C-0950.

DDC FILE COPY

APPROVED FOR PUBLIC RELEASE; DISTRIBUTION UNLIMITED

DDC
JAN 17 1979

✓

DOUGLAS AIRCRAFT COMPANY

MCDONNELL DOUGLAS



79 01 16 158

Copy number

Report number

MDC J7998

A GENERAL METHOD FOR CALCULATING THREE-DIMENSIONAL
LAMINAR AND TURBULENT BOUNDARY LAYERS
ON SHIP HULLS

Revision date

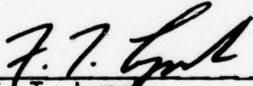
Revision letter

Issue date October 1978

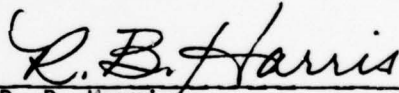
Contract number N00014-76-C-0950

Prepared by: Tuncer Cebeci, K. C. Chang and Kalle Kaups

Approved by:



F. T. Lynch
Branch Chief
Research & Development
Aerodynamics Subdivision



R. B. Harris
Chief Technology Engineer
Aerodynamics

This research was carried out under the Naval Sea Systems Command General Hydrodynamics Research program subproject SR 023 01 01, administered by the David W. Taylor Naval Ship Research and Development Center under contract N00014-76-C-0950.

| | |
|---------------------------------|---|
| ACQUISITION BY | |
| DTIC | White Section <input checked="" type="checkbox"/> |
| DDC | Red Section <input type="checkbox"/> |
| UNCLASSIFIED | <input type="checkbox"/> |
| JUSTIFICATION | |
| BY | |
| DISTRIBUTION/AVAILABILITY CODES | |
| AVAIL. AND/OR SPECIAL | |
| A | |

DOUGLAS AIRCRAFT COMPANY

MCDONNELL DOUGLAS



79 01 16 158

Report No. MDC J7998

A GENERAL METHOD FOR CALCULATING THREE-DIMENSIONAL LAMINAR
AND TURBULENT BOUNDARY LAYERS ON SHIP HULLS

by

Tuncer Cebeci, K. C. Chang and Kalle Kaups

October 1978

This research was carried out under the Naval Sea Systems
Command General Hydromechanics Research Program subproject
SR 023 01 01, administered by the David W. Taylor Naval
Ship Research and Development Center under contract
N00014-76-C-0950.

Approved for public release; distribution unlimited.

ABSTRACT

A general method for representing the flow properties in the three-dimensional boundary layers around ship hulls of arbitrary shape is described. It makes use of an efficient two-point finite-difference scheme to solve the boundary-layer equations and includes an algebraic eddy-viscosity representation of the Reynolds-stress tensor. The numerical method contains novel and desirable features and allows the calculation of flows in which the circumferential velocity component contains regions of flow reversal across the boundary layer. The inviscid pressure distribution is determined with the Douglas-Neumann method which, if necessary, can conveniently allow for the boundary-layer displacement surface. To allow its application to ships, and particularly to those with double-elliptic and flat-bottomed hulls, a non-orthogonal coordinate system has been developed and is shown to be economical, precise and comparatively easy to use. Present calculations relate to zero Froude number but they can be extended to include the effects of a water wave and local regions of flow separation which may stem from bulbous-bow geometries.

TABLE OF CONTENTS

| | Page |
|---|------|
| I. Introduction | 1 |
| II. Basic Equations | 3 |
| 2.1 The Boundary-Layer Equations | 3 |
| 2.2 Initial Conditions | 4 |
| 2.3 Turbulence Model | 7 |
| 2.4 Transformation of the Basic Equations | 8 |
| III. Coordinate System | 12 |
| IV. Numerical Method | 17 |
| 4.1 Difference Equations for the Longitudinal Attachment- Line Equations | 17 |
| 4.2 Difference Equations for the Full Three-Dimensional Equations | 20 |
| 4.3 Solution of the Difference Equations | 21 |
| V. Results | 26 |
| 5.1 Turbulent Flow Calculations for a Curved Duct and Comparison with Experiment | 26 |
| 5.2 Results for a Double Elliptic Ship Model | 31 |
| 5.3 Results of Ship Model 5350 | 39 |
| VI. Concluding Remarks and Future Work | 46 |
| 6.1 Generation of Initial Conditions on Arbitrary Bow Configurations | 46 |
| 6.2 Viscous-Inviscid Flow Interaction | 48 |
| 6.3 Prediction of Wake Behind Ship Hulls | 48 |
| VII. Acknowledgment | 49 |
| VIII. References | 50 |
| Appendix A. Description of the Boundary-Layer Computer Program . . . | 52 |

| | | |
|-----|---|----|
| A.1 | Input for the Geometry Program | 53 |
| A.2 | Input for the Boundary-Layer Program | 55 |
| A.3 | Output for the Geometry Program | 56 |
| A.4 | Output for the Boundary-Layer Program | 57 |

LIST OF FIGURES

| Number | Title | Page |
|--------|--|------|
| 1. | The nonorthogonal coordinate system and the initial data lines for the ship hull | 5 |
| 2. | Notation of corner points used in the mapping procedure . . . | 14 |
| 3. | Resolution of the velocity components | 16 |
| 4. | Net rectangle for the longitudinal attachment-line equations | 18 |
| 5. | New cube for the difference equations for three-dimensional flows, $\omega_j > 0$ | 21 |
| 6. | Coordinate system and notation for the curved duct | 26 |
| 7. | Comparison of generated initial total velocity profiles with Vermulen's data | 29 |
| 8. | Comparison of computed momentum thickness with Vermulen's data | 30 |
| 9. | Comparison of computed shape factor with Vermulen's data . . | 30 |
| 10. | Comparison of computed skin friction coefficient with Vermulen's data | 30 |
| 11. | Comparison of computed limiting crossflow angle with Vermulen's data | 30 |
| 12. | Comparison of computed total velocity profiles with Vermulen's data | 32 |
| 13. | Comparison of computed crossflow angle with Vermulen's data . | 33 |
| 14. | Three-dimensional picture of double elliptic ship model with the nonorthogonal coordinate system | 33 |
| 15. | Pressure distribution for the double-elliptic ship | 34 |
| 16. | Computed c_p , c_f , H_{11} , B_θ and β_w for the double-elliptic ship model for $R_L = 10^7$ at (a) $x/L = -0.85$, (b) $x/L = -0.50$, (c) $x/L = 0.0$, (d) $x/L = 0.25$, (e) $x/L = 0.50$, (f) $x/L = 0.75$ | 35 |
| 17. | Computed longitudinal and transverse velocity profiles for the double-elliptic ship model for $R_L = 10^7$ at $z = 0.6$. | 38 |

| Number | Title | Page |
|--------|--|------|
| 18. | Computed transverse velocity profiles for the double-elliptic ship model at $x/L = -0.2$ | 39 |
| 19. | Three-dimensional view of ship model 5350 with the nonorthogonal coordinate system | 40 |
| 20. | Body plan for ship model 5350 | 40 |
| 21. | Pressure distribution for the entire ship model 5350 | 41 |
| 22. | Pressure distribution for the bow region of ship model 5350 | 41 |
| 23. | Computed c_p , c_f , H_{11} , R_θ and β_w for ship model 5350 for $R_L = 3 \times 10^8$ at (a) $x = 30m$, (b) $x = 60m$, (c) $x = 105m$, (d) $x = 165m$, (e) $x = 210m$ | 42 |
| 24. | Computed streamwise velocity profiles for ship model 5350 for $R_L = 3 \times 10^8$ along (a) $z = 0.2$ and (b) $x = 105m$ coordinate lines | 44 |
| 25. | Computed crosswise velocity profiles for ship model 5350 for $R_L = 3 \times 10^8$ along $x = 60m$ coordinate line | 45 |
| 26. | Pattern of streamlines near the bow of ship model 5350 | 46 |
| A.1 | Basic flow chart for the boundary-layer program | 60 |

PRINCIPAL NOTATION

| | |
|--|---|
| A | Van Driest damping parameter, see (2.18b) |
| A_1, A_2, A_3, A_4 | constants |
| c_f | local skin-friction coefficient in streamwise direction |
| C_1, C_2, C_3, C_4 | constants |
| f | transformed vector potential for ψ |
| g | transformed vector potential for ϕ |
| h_1, h_2 | metric coefficients |
| h_j | net spacing in η -direction |
| H, H_{11} | boundary-layer shape factor along streamwise direction, δ^*/θ_{11} |
| k_n | net spacing in x -direction |
| K_1, K_2 | geodesic curvatures, see (2.5) |
| K_{12}, K_{21} | geometric parameters, see (2.6) |
| L | mixing length, see (2.18a), or reference length |
| m_1, m_2, \dots, m_{12} | coefficients, see (2.28) or (2.32) |
| p | static pressure |
| Q | total velocity in the boundary layer |
| R_x, R_L | Reynolds numbers, $u_e s_1/\nu$ and $u_\infty L/\nu$ |
| R_{δ^*} | Reynolds number, $u_{se} \delta^*/\nu$ |
| R_θ | Reynolds number, $u_{se} \theta_{11}/\nu$ |
| s | arc length along coordinate line |
| \hat{e}_1, \hat{e}_2 | unit tangent vectors along x and z directions |
| u, v, w | velocity components in the x, y, z directions |
| $\bar{u}, \bar{v}, \bar{w}$ | velocity components in the Cartesian coordinate |
| u_s, u_n | velocity components in boundary layer parallel and normal, respectively, to external streamline |
| u_τ | friction velocity, see (2.18c) |
| u_∞ | freestream velocity |
| u_{ref} | reference velocity |
| x, y, z | nonorthogonal boundary-layer coordinates |
| $\bar{x}, \bar{y}, \bar{z}$ | Cartesian coordinates |
| $-\rho \overline{u'v'}, -\rho \overline{v'w'}$ | Reynolds stresses |
| β | crossflow angle |

| | |
|----------------|--|
| β_w | limiting crossflow angle |
| δ | boundary-layer thickness |
| δ^* | displacement thickness, $\int_0^{\infty} (1 - u_s/u_{se}) dy$ |
| ϵ_m | eddy viscosity |
| ϵ_m^+ | dimensionless eddy viscosity, ϵ_m/ν |
| n | similarity variable for y , see (2.21) |
| θ_{11} | momentum thickness, $\int_0^{\infty} u_s/u_{se} (1 - u_s/u_{se}) dy$ |
| μ | dynamic viscosity |
| ν | kinematic viscosity |
| ρ | density |
| τ | shear stress |
| ϕ, ψ | two-component vector potentials, see (2.23) |

Subscripts

| | |
|-----|----------------------|
| e | boundary-layer edge |
| s | streamwise direction |
| t | total value |
| w | wall |

primes denote differentiation with respect to n

I. INTRODUCTION

A general method for determining the local flow properties and the overall drag on ship hulls is very desirable and particularly so with the present need to conserve energy resources. It is difficult to achieve for a number of reasons including the turbulent nature of the three-dimensional boundary layer, the complexity and wide range of geometrical configurations employed, the possibility of local regions of separated flow and the existence of the free surface. In addition, and although these difficulties may be overcome in total or in part, the resulting calculation method must have the essential features of generality, efficiency and accuracy.

The purpose of this report is to describe a general method which is capable of representing the flow properties in the boundary layer around ship hulls of arbitrary shape. It is based on the general method of Cebeci, Kaups and Ramsey¹, developed for calculating three-dimensional, compressible laminar and turbulent boundary layers on arbitrary wings and previously proved to satisfy the requirements of numerical economy and precision. To allow its application to ships in general, and to double-elliptic and flat-bottomed hulls in particular, an appropriate coordinate system has been developed. Previously described coordinate systems, for example a streamline system such as that of Lin and Hall² or the orthogonal arrangement of Miloh and Patel³ are limited in their applicability and the present nonorthogonal arrangement is similar to that of Cebeci, Kaups and Ramsey¹.

The numerical procedure for solving the three-dimensional boundary-layer equations makes use of Keller's two-point finite-difference method⁴ and Cebeci and Stewartson's procedure in computing flows in which the transverse velocity component contains regions of reverse flow. This is in contrast to previous investigations, for example those of Lin and Hall² and Gadd⁵ which are limited either to zero crossflow or to a unidirectional and small crossflow. It is also in contrast to the previous methods of Chang and Patel⁶ and Cebeci and Chang⁷ which did not have a good and reliable procedure for computing the flow in which the transverse velocity component contained flow reversal.

In representing turbulent flow by time-averaged equations, a turbulence model is required and an algebraic eddy-viscosity formulation, similar to that of Cebeci, Kaups and Ramsey¹, is used. This is in contrast to the two-equation approach which Rastogi and Rodi⁸ have applied to three-dimensional boundary layers and which, in principle, should be better able to represent flows which are far from equilibrium. The previous comparisons presented in Cebeci^{9,10} demonstrated that the present eddy-viscosity model allows excellent agreement between measurements and calculations but did not include comparison with the three-dimensional boundary-layer measurements of Vermeulen¹¹. Since this data includes a strongly adverse-pressure gradient case which allows a stringent test of the present model, corresponding calculations and comparisons are reported.

The calculation method is described in detail in the following section which states the three-dimensional boundary-layer equations in curvilinear nonorthogonal coordinates and describes and discusses the required initial conditions, turbulence model and transformations in separate subsections. Section 3 is devoted to the coordinate system which is an essential feature of the present method. The numerical method is discussed briefly in section 4 and calculated results are presented in section 5 which includes comparisons with the measurements of Vermeulen¹¹ and demonstrations of the ability of the method to represent the geometry of different hull configurations and to result in realistic velocity and drag characteristics. Summary conclusions are presented in section 6. Finally, in Appendix A we present a description of the computer program.

II. BASIC EQUATIONS

2.1 The Boundary-Layer Equations

The governing boundary-layer equations for three-dimensional incompressible laminar and turbulent flows in a curvilinear nonorthogonal coordinate system are given by:

Continuity Equation

$$\frac{\partial}{\partial x} (uh_2 \sin\theta) + \frac{\partial}{\partial z} (wh_1 \sin\theta) + \frac{\partial}{\partial y} (vh_1h_2 \sin\theta) = 0 \quad (2.1)$$

x-Momentum Equation

$$\begin{aligned} \frac{u}{h_1} \frac{\partial u}{\partial x} + \frac{w}{h_2} \frac{\partial u}{\partial z} + v \frac{\partial u}{\partial y} - K_1 u^2 \cot\theta + K_2 w^2 \csc\theta + K_{12} uw \\ = - \frac{\csc^2\theta}{h_1} \frac{\partial}{\partial x} \left(\frac{P}{\rho} \right) + \frac{\cot\theta \csc\theta}{h_2} \frac{\partial}{\partial z} \left(\frac{P}{\rho} \right) + \frac{\partial}{\partial y} \left(v \frac{\partial u}{\partial y} - \overline{u'v'} \right) \end{aligned} \quad (2.2)$$

z-Momentum Equation

$$\begin{aligned} \frac{u}{h_1} \frac{\partial w}{\partial x} + \frac{w}{h_2} \frac{\partial w}{\partial z} + v \frac{\partial w}{\partial y} - K_2 w^2 \cot\theta + K_1 u^2 \csc\theta + K_{21} uw \\ = \frac{\cot\theta \csc\theta}{h_1} \frac{\partial}{\partial x} \left(\frac{P}{\rho} \right) - \frac{\csc^2\theta}{h_2} \frac{\partial}{\partial z} \left(\frac{P}{\rho} \right) + \frac{\partial}{\partial y} \left(v \frac{\partial w}{\partial y} - \overline{v'w'} \right) \end{aligned} \quad (2.3)$$

Here h_1 and h_2 are the metric coefficients and they are, in general, functions of x and z ; that is,

$$h_1 = h_1(x, z); \quad h_2 = h_2(x, z) \quad (2.4)$$

Also, θ represents the angle between the coordinates x and z . The parameters K_1 and K_2 are known as the geodesic curvatures of the curves $z = \text{const}$ and $x = \text{const}$, respectively. They are given by

$$\begin{aligned} K_1 &= \frac{1}{h_1 h_2 \sin\theta} \left[\frac{\partial}{\partial x} (h_2 \cos\theta) - \frac{\partial h_1}{\partial z} \right], \\ K_2 &= \frac{1}{h_1 h_2 \sin\theta} \left[\frac{\partial}{\partial z} (h_1 \cos\theta) - \frac{\partial h_2}{\partial x} \right] \end{aligned} \quad (2.5)$$

The parameters K_{12} and K_{21} are defined by

$$K_{12} = \frac{1}{\sin\theta} \left[-\left(K_1 + \frac{1}{h_1} \frac{\partial\theta}{\partial x} \right) + \cos\theta \left(K_2 + \frac{1}{h_2} \frac{\partial\theta}{\partial z} \right) \right] \quad (2.6a)$$

$$K_{21} = \frac{1}{\sin\theta} \left[-\left(K_2 + \frac{1}{h_2} \frac{\partial\theta}{\partial z} \right) + \cos\theta \left(K_1 + \frac{1}{h_1} \frac{\partial\theta}{\partial x} \right) \right] \quad (2.6b)$$

For an orthogonal system $\theta = \pi/2$ and the parameters K_1 , K_2 , K_{12} and K_{21} , reduce to

$$K_1 = -\frac{1}{h_1 h_2} \frac{\partial h_1}{\partial z}, \quad K_2 = -\frac{1}{h_1 h_2} \frac{\partial h_2}{\partial x} \quad (2.7)$$

$$K_{12} = -K_1 \quad K_{21} = -K_2 \quad (2.8)$$

At the edge of the boundary layer, (2.2) and (2.3) reduce to

$$\begin{aligned} \frac{u_e}{h_1} \frac{\partial u_e}{\partial x} + \frac{w_e}{h_2} \frac{\partial u_e}{\partial z} - K_1 u_e^2 \cot\theta + K_2 w_e^2 \csc\theta + K_{12} u_e w_e \\ = -\frac{\csc^2\theta}{h_1} \frac{\partial}{\partial x} \left(\frac{P}{\rho} \right) + \frac{\cot\theta \csc\theta}{h_2} \frac{\partial}{\partial z} \left(\frac{P}{\rho} \right) \end{aligned} \quad (2.9)$$

$$\begin{aligned} \frac{u_e}{h_1} \frac{\partial w_e}{\partial x} + \frac{w_e}{h_2} \frac{\partial w_e}{\partial z} - K_2 w_e^2 \cot\theta + K_1 u_e^2 \csc\theta + K_{21} u_e w_e \\ = \frac{\cot\theta \csc\theta}{h_1} \frac{\partial}{\partial x} \left(\frac{P}{\rho} \right) - \frac{\csc^2\theta}{h_2} \frac{\partial}{\partial z} \left(\frac{P}{\rho} \right) \end{aligned} \quad (2.10)$$

The boundary conditions for equations (2.1) and (2.3) are:

$$y = 0 : \quad u, v, w = 0 \quad (2.11a)$$

$$y = \delta : \quad u = u_e(x, z), \quad w = w_e(x, z) \quad (2.11b)$$

2.2 Initial Conditions

The solution of the system given by (2.1) to (2.3), subject to (2.11), requires initial conditions on two planes intersecting the body along coordinate

lines. In general, the construction of these initial conditions for three-dimensional flows on arbitrary bodies such as ship hulls is difficult due to the variety of bow shapes which may be extensive and complicated. For this reason, assumptions are necessary for them in order to start the calculations.

In our study we choose the inviscid dividing streamline on which $\partial p / \partial z = 0$ to be one of the initial data line (see figure 1). In the case

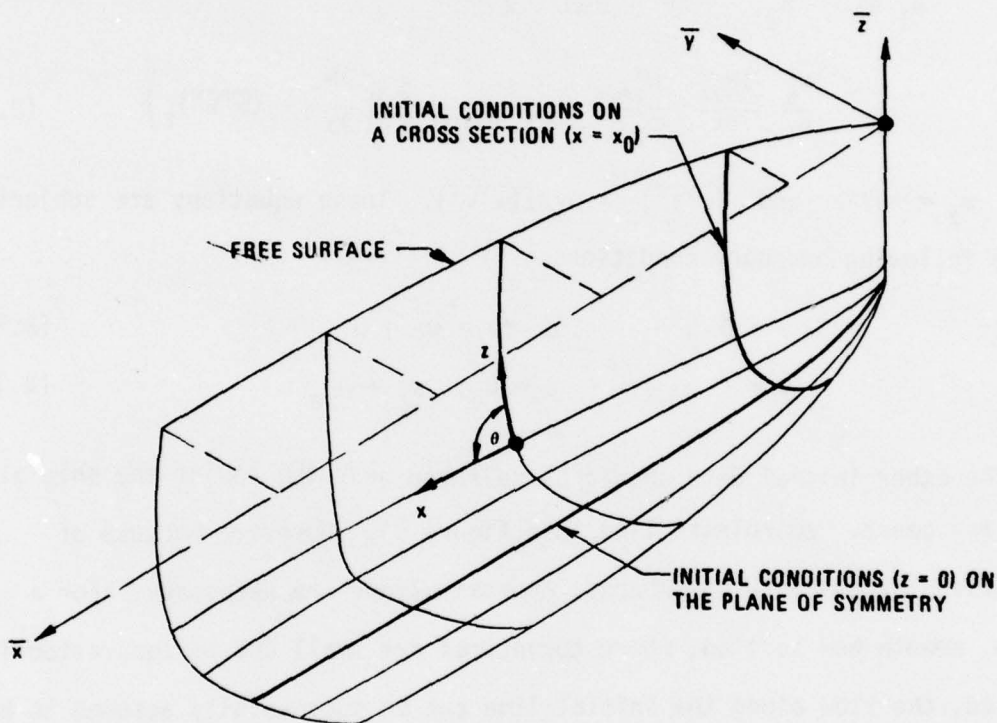


Figure 1. The nonorthogonal coordinate system and the initial data lines for the ship hull.

of a rectilinear motion of a ship, this streamline runs along the plane of symmetry. Because of symmetry conditions w and $\partial p / \partial z$ are zero on this line causing (2.3) to become singular. However, differentiation with respect to z yields a nonsingular equation. After performing the necessary differentiation for the z -momentum equation and taking advantage of appropriate symmetry conditions, we can write the so-called longitudinal attachment-line equations as:

Continuity Equation

$$\frac{\partial}{\partial x} (u h_2 \sin \theta) + h_1 \sin \theta w_z + \frac{\partial}{\partial y} (v h_1 h_2 \sin \theta) = 0 \quad (2.12)$$

x-Momentum Equation

$$\frac{u}{h_1} \frac{\partial u}{\partial x} + v \frac{\partial u}{\partial y} - \cot \theta K_1 u^2 = \frac{u_e}{h_1} \frac{\partial u_e}{\partial x} - K_1 u_e^2 \cot \theta + \frac{\partial}{\partial y} \left(\nu \frac{\partial u}{\partial y} - \overline{u'v'} \right) \quad (2.13)$$

z-Momentum Equation

$$\begin{aligned} \frac{u}{h_1} \frac{\partial w_z}{\partial x} + \frac{w_z^2}{h_2} + v \frac{\partial w_z}{\partial y} + K_{21} u w_z \\ = \frac{u_e}{h_1} \frac{\partial w_{ze}}{\partial x} + \frac{w_{ze}^2}{h_2} + K_{21} u_e w_{ze} + \frac{\partial}{\partial y} \left(\nu \frac{\partial w_z}{\partial y} - (\overline{w'v'})_z \right) \end{aligned} \quad (2.14)$$

where $w_z = \partial w / \partial z$ and $(\overline{w'v'})_z = \partial / \partial z (\overline{w'v'})$. These equations are subject to the following boundary conditions:

$$y = 0 : \quad u = v = w_z = 0 \quad (2.15a)$$

$$y = \delta : \quad u = u_e, \quad w_z = w_{ze} \quad (2.15b)$$

The other initial data should be selected near the bow of the ship along some $x = \text{const.}$ coordinate line (see figure 1). However, because of the variety of possible bow shapes, approximations are necessary. For a simple, smooth bow section, where curvatures are small and no separation is expected, the flow along the initial line can be successfully assumed to be two-dimensional without pressure gradient, and the governing two-dimensional equations for a flat plate are solved. However, for most general merchant ships, the bow section is complicated and flow separation and reattachment are expected because of large curvature variations and adverse pressure gradients; as a consequence, the boundary-layer calculations can only be performed downstream of the reattachment line (or point) where turbulent flow is presumed (since it is unlikely that the flow remains laminar after separation and reattachment with high Reynolds number). Generation of the initial data for turbulent flows is much more involved if there are no

experimental data available. It requires sound mathematical and physical judgment and tedious trial-and-error efforts. We shall discuss this aspect of the problem later in the report.

2.3 Turbulence Model

For turbulent flows, it is necessary to make closure assumptions for the Reynolds stresses, $-\rho \overline{u'v'}$ and $-\rho \overline{v'w'}$. In our study, we satisfy the requirement by using the eddy-viscosity concept and relate the Reynolds stresses to the mean velocity profiles by

$$-\overline{u'v'} = \epsilon_m \frac{\partial u}{\partial y}, \quad -\overline{v'w'} = \epsilon_m \frac{\partial w}{\partial y} \quad (2.16)$$

We use the eddy-viscosity formulation of Cebeci⁹, and define ϵ_m by two separate formulas. In the inner region, ϵ_m is defined as

$$(\epsilon_m)_i = L^2 \left[\left(\frac{\partial u}{\partial y} \right)^2 + \left(\frac{\partial w}{\partial y} \right)^2 + 2 \cos \theta \left(\frac{\partial u}{\partial y} \right) \left(\frac{\partial w}{\partial y} \right) \right]^{1/2} \quad (2.17)$$

where

$$L = 0.4 y [1 - \exp(-y/A)] \quad (2.18a)$$

$$A = 26 \frac{\nu}{u_\tau}, \quad u_\tau = \left(\frac{\tau_{tw}}{\rho} \right)^{1/2} \quad (2.18b)$$

$$\tau_{tw} = \mu \left[\left(\frac{\partial u}{\partial y} \right)_w^2 + \left(\frac{\partial w}{\partial y} \right)_w^2 + 2 \cos \theta \left(\frac{\partial u}{\partial y} \right)_w \left(\frac{\partial w}{\partial y} \right)_w \right]^{1/2} \quad (2.18c)$$

In the outer region ϵ_m is defined by the following formula

$$\epsilon_m = 0.0168 \left| \int_0^\infty (u_{te} - u_t) dy \right| \quad (2.19)$$

where

$$u_{te} = (u_e^2 + w_e^2 + 2u_e w_e \cos \theta)^{1/2} \quad (2.20a)$$

$$u_t = (u^2 + w^2 + 2uw \cos\theta)^{1/2} \quad (2.20b)$$

The inner and outer regions are established by the continuity of the eddy-viscosity formula.

2.4 Transformation of the Basic Equations

The boundary-layer equations can be solved either in physical coordinates or in transformed coordinates. Each coordinate system has its own advantage. In three-dimensional flows, the computer time and storage required is an important factor. The transformed coordinates are then favored because the coordinates allow larger steps to be taken in the longitudinal and transverse directions.

We define the transformed coordinates by

$$x = x, \quad z = z, \quad d\eta = \left(\frac{u_e}{vs_1}\right)^{1/2} dy, \quad s_1 = \int_0^x h_1 dx \quad (2.21)$$

and introduce a two-component vector potential such that

$$uh_2 \sin\theta = \frac{\partial\psi}{\partial y}, \quad wh_1 \sin\theta = \frac{\partial\phi}{\partial y} \quad (2.22a)$$

$$vh_1 h_2 \sin\theta = -\left(\frac{\partial\psi}{\partial x} + \frac{\partial\phi}{\partial z}\right) \quad (2.22b)$$

where ψ and ϕ are defined by

$$\psi = (vs_1 u_e)^{1/2} h_2 \sin\theta f(x, z, \eta) \quad (2.23a)$$

$$\phi = (vs_1 u_e)^{1/2} u_{ref}/u_e h_1 \sin\theta g(x, z, \eta) \quad (2.23b)$$

and u_{ref} is some reference velocity.

Using these transformations and the relations given by (2.9), (2.10) and (2.11), we can write the x-momentum and z-momentum equations for the general case as

x-Momentum

$$\begin{aligned} & (bf'')' + m_1 ff'' - m_2 (f')^2 - m_5 f'g' + m_6 f''g - m_8 (g')^2 + m_{11} \\ & = m_{10} \left(f' \frac{\partial f'}{\partial x} - f'' \frac{\partial f}{\partial x} \right) + m_7 \left(g' \frac{\partial f'}{\partial z} - f'' \frac{\partial g}{\partial z} \right) \end{aligned} \quad (2.24)$$

z-Momentum

$$\begin{aligned} & (bg'')' + m_1 fg'' - m_4 f'g' - m_3 (g')^2 + m_6 gg'' - m_9 (f')^2 + m_{12} \\ & = m_{10} \left(f' \frac{\partial g'}{\partial x} - g'' \frac{\partial f}{\partial x} \right) + m_7 \left(g' \frac{\partial g'}{\partial z} - g'' \frac{\partial g}{\partial z} \right) \end{aligned} \quad (2.25)$$

and their boundary conditions as

$$\eta = 0: f = f' = g = g' = 0; \quad \eta = \eta_\infty, f' = 1, g' = w_e/u_{\text{ref}} \quad (2.26)$$

Here primes denote differentiation with respect to η , and

$$f' = \frac{u}{u_e}, \quad g' = \frac{w}{u_{\text{ref}}}, \quad b = 1 + \epsilon_m^+, \quad \epsilon_m^+ = \frac{\epsilon_m}{v} \quad (2.27)$$

The coefficients m_1 to m_{12} are given by

$$\begin{aligned} m_1 &= \frac{1}{2} \left(1 + \frac{s_1}{h_1 u_e} \frac{\partial u_e}{\partial x} \right) + \frac{s_1}{h_1 h_2 \sin \theta} \frac{\partial}{\partial x} (h_2 \sin \theta) \\ m_2 &= \frac{s_1}{h_1 u_e} \frac{\partial u_e}{\partial x} - s_1 K_1 \cot \theta, \quad m_3 = -s_1 K_2 \frac{u_{\text{ref}}}{u_e} \cot \theta \\ m_4 &= s_1 K_{21}, \quad m_5 = \frac{s_1}{h_2} \frac{u_{\text{ref}}}{u_e^2} \frac{\partial u_e}{\partial z} + s_1 K_{12} \frac{u_{\text{ref}}}{u_e} \\ m_6 &= \frac{s_1}{h_1 h_2 \sin \theta} \frac{1}{\sqrt{u_e s_1}} \frac{\partial}{\partial z} \left(\sqrt{u_e s_1} h_1 \sin \theta \frac{u_{\text{ref}}}{u_e} \right) \\ m_7 &= \frac{s_1}{h_2} \frac{u_{\text{ref}}}{u_e}, \quad m_8 = s_1 K_2 \left(\frac{u_{\text{ref}}}{u_e} \right)^2 \csc \theta \\ m_9 &= s_1 K_1 \csc \theta \frac{u_e}{u_{\text{ref}}}, \quad m_{10} = \frac{s_1}{h_1} \\ m_{11} &= m_2 + m_5 \frac{w_e}{u_{\text{ref}}} + m_8 \left(\frac{w_e}{u_{\text{ref}}} \right)^2 \end{aligned} \quad (2.28)$$

$$m_{12} = m_4 \frac{w_e}{u_{ref}} + m_3 \left(\frac{w_e}{u_{ref}} \right)^2 + m_9 + \frac{m_{10}}{u_{ref}} \frac{\partial w_e}{\partial x} + \frac{m_7 w_e}{u_{ref}^2} \frac{\partial w_e}{\partial z}$$

To transform the longitudinal attachment-line flow equations and the boundary conditions, we use the transformed coordinates given by (2.21) and define the two-component vector potential by

$$uh_2 \sin\theta = \frac{\partial \psi}{\partial y} \quad , \quad w_z h_1 \sin\theta = \frac{\partial \phi}{\partial y} \quad (2.29)$$

$$vh_1 h_2 \sin\theta = - \left(\frac{\partial \psi}{\partial x} + \phi \right)$$

with ϕ and ψ still given by (2.23). With these variables, the longitudinal attachment-line equations in the transformed coordinates can be written as

$$(bf'')' + m_1 f f'' - m_2 (f')^2 + m_6 f'' g + m_{11} = \frac{s_1}{h_1} \left(f' \frac{\partial f'}{\partial x} - f'' \frac{\partial f}{\partial x} \right) \quad (2.30)$$

$$\begin{aligned} (bg'')' + m_1 g'' f - m_4 f' g' - m_3 (g')^2 + m_6 g g'' - m_9 (f')^2 + m_{12} \\ = \frac{s_1}{h_1} \left(f' \frac{\partial g'}{\partial x} - g'' \frac{\partial f}{\partial x} \right) \end{aligned} \quad (2.31)$$

The boundary conditions and the coefficients m_1 to m_{12} are the same as in (2.26) and in (2.28) except now

$$\begin{aligned} n = n_\infty; \quad g' = \frac{w_{ze}}{u_{ref}} \\ m_3 = \frac{s_1}{h_2} \frac{u_{ref}}{u_e} \quad , \quad m_6 = m_3 \\ m_9 = 0 \quad , \quad m_{11} = m_2 \\ m_{12} = m_3 \left(\frac{w_{ze}}{u_{ref}} \right)^2 + m_4 \frac{w_{ze}}{u_{ref}} + \frac{s_1}{h_1} \frac{1}{u_{ref}} \frac{\partial w_{ze}}{\partial x} \end{aligned} \quad (2.32)$$

In terms of the transformed variables, the algebraic eddy-viscosity formulas as given by (2.17) to (2.20) become

$$(\epsilon_m)_i = \frac{1}{\sqrt{R_x}} n^2 \left[1 - \exp\left(-\frac{y}{\lambda}\right) \right]^2 \left[(f'')^2 + \left(\frac{u_{ref}}{u_e} \right)^2 (g'')^2 + 2 \cos\theta \frac{u_{ref}}{u_e} f'' g'' \right]^{1/2} \quad (2.33)$$

$$(\epsilon_m)_0 = 0.0168 \sqrt{R_x} \int_0^{\eta_{\infty}} \left\{ \left[1 + \left(\frac{w_e}{u_e} \right)^2 + 2 \left(\frac{w_e}{u_e} \right) \cos \theta \right]^{\frac{1}{2}} \right. \\ \left. - \left[(f')^2 + \left(\frac{u_{\text{ref}}}{u_e} \right)^2 (g')^2 + 2 \frac{u_{\text{ref}}}{u_e} \cos \theta f' g' \right]^{\frac{1}{2}} \right\} d\eta$$

Here $R_x = u_e s_1 / \nu$ and

$$\frac{\gamma}{A} = \frac{R_x^{\frac{1}{4}}}{26} \eta \left[(f''_w)^2 + \left(\frac{u_{\text{ref}}}{u_e} \right)^2 (g''_w)^2 + 2 \cos \theta \frac{u_{\text{ref}}}{u_e} f''_w g''_w \right]^{\frac{1}{4}}$$

III. COORDINATE SYSTEM

Since, in general, a ship hull is a complicated nondevelopable surface, a Cartesian coordinate system is not suitable for boundary-layer calculations. Most existing merchant and naval vessels possess the following features: a flat bottom [$\bar{y} = f(\bar{x}, \bar{z})$ is not a single-valued function]; a bottom which is not parallel to the water surface; and a bow which has a submerged bulb extending toward the origin. In addition, the problem is further complicated by the existence of a free surface, corresponding to the water level of a partly-submerged hull. The chosen coordinate system must be sufficiently general to allow these various features to be represented in the boundary-layer calculations.

The streamline coordinate system is superficially attractive but the determination of the streamlines, the orthogonal lines, and the associated geometrical parameters requires considerable effort. They are dependent on the Froude number, and also on the Reynolds number if the displacement effect is taken into account. Consequently, and in addition to being hard to compute, this coordinate system becomes uneconomical to use when the effect of the Froude number and the Reynolds number are to be systematically examined.

A desirable requirement of a coordinate system for the boundary-layer calculations, is that it be calculated only once. Miloh and Patel³ proposed an orthogonal coordinate system which depends only on the body geometry and is calculated once and for all. This coordinate system has been applied by Chang and Patel⁶ to boundary-layer calculations on two simple ship hulls: ellipsoid and double elliptic ship. One of the coordinates is taken as lines of $x = \bar{x} = \text{constant}$ and the other as $z(\bar{x}, \bar{z}) = \text{constant}$, which is orthogonal to $x = \text{constant}$ lines everywhere on the ship hull, and is obtained from the solution of the differential equation

$$\frac{d\bar{z}}{d\bar{x}} = - \frac{f_{\bar{x}} f_{\bar{z}}}{1 + f_{\bar{z}}^2} \quad (3.1)$$

Here $\bar{y} = f(\bar{x}, \bar{z})$ defines the ship hull, and $(\bar{x}, \bar{y}, \bar{z})$ denote the Cartesian coordinates. The major advantage of this coordinate system is its simplicity. Because one of the coordinates is subject to the condition (3.1), there is no

guarantee that the boundaries of the ship hull are coincident with the coordinate lines. Furthermore, for a ship with flat bottom for which $\bar{y} = f(\bar{x}, \bar{z})$ is not a single-valued function, one of the coordinates cannot be calculated from (3.1). The coordinate system is limited, therefore, to some special geometries only.

In this study we adopt a nonorthogonal coordinate system similar to that developed by Cebeci, Kaups and Ramsey¹ for arbitrary wings. It is based on body geometries only and, hence, it is calculated once and for all. In addition, the system can deal with the peculiar features of most merchant and naval vessels discussed previously. The details of this coordinate system are described briefly in the following paragraph.

Now consider the ship hull as given in the usual Cartesian coordinate system; that is, \bar{x} along the ship axis, \bar{y} and \bar{z} in the crossplane (see figure 1). We select $x = \bar{x} = \text{constant}$ as one of the coordinates and the other coordinate z lies in the $\bar{y}\bar{z}$ -plane. Because the coordinate system is nonorthogonal, we are free to select the values of z in the plane to satisfy the condition that the boundary lines of the ship hull are coincident with $z = \text{constant}$ coordinate lines. There are several ways of defining the z -values. Here z is determined by mapping each $\bar{y}\bar{z}$ crossplane into a half or full unit circle depending on whether the crossplane intercepts the free surface or is completely submerged. The polar angle, normalized by π or 2π on the unit circle, is taken as z -values. The z -values then range from 0 to 1 on each crossplane. The advantage of the mapping method is that equi-interval, $z = \text{constant}$ coordinate lines are automatically concentrated in the region of large curvature where the boundary-layer characteristics are expected to vary greatly. Hence the number of $z = \text{constant}$ coordinate lines can be reduced without loss of accuracy.

There are several methods available for the mapping of an arbitrary body onto a unit circle. Here we use the numerical mapping method developed by Halsey¹². It makes full use of Fast Fourier Transform techniques and has no restrictions on the shape of the body to be mapped. To map a smooth crossplane onto a unit circle, the procedure is fairly easy. If there are inner corner points, or trailing-edge and leading-edge corner points (see figure 2) caused by the reflection of the crossplane, they must be removed before mapping

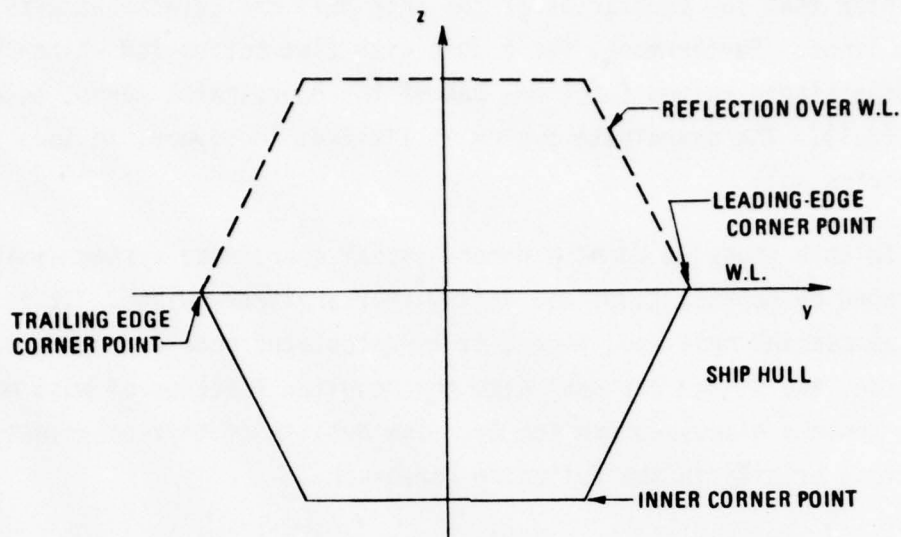


Figure 2. Notation of corner points used in the mapping procedure.

is performed to improve numerical accuracy and to provide rapid convergence. The inner corner points are rounded off by using Fourier series expansion technique and the leading-edge and/or trailing-edge corner points and removed by using the Karman-Trefftz mapping. For details see Halsey¹².

To use the mapping method to find the coordinate system, it is only necessary to define the ship hull as a family of points in the $x=\text{constant}$ planes, to locate the intersection of the ship hull and the free surface, and to indicate whether corner points exist. The data in each plane is then mapped into a unit circle as \bar{y} vs z and \bar{z} vs z and interpolated for constant values of z . Another set of spline fits in the planes $z=\text{constant}$ for \bar{y} vs x and \bar{z} vs x completes the definition of the coordinate system. The lines formed by the intersection of the planes $x=\text{constant}$ and $z=\text{constant}$ with the hull constitute the nonorthogonal coordinate net on the surface, and the third boundary-layer coordinate is taken as the distance normal to the surface in accordance with first-order boundary-layer approximation.

Since the spline-fitting also yields derivatives, the metric coefficient and the geodesic curvatures of the coordinate lines can be calculated from the formulas given below.

The metric coefficients:

$$h_1^2 = 1 + \left(\frac{\partial \bar{z}}{\partial x}\right)_z^2 + \left(\frac{\partial \bar{y}}{\partial x}\right)_z^2 \quad (3.2a)$$

$$h_2^2 = \left(\frac{\partial \bar{y}}{\partial z}\right)_x^2 + \left(\frac{\partial \bar{z}}{\partial z}\right)_x^2 \quad (3.2b)$$

The angle between the coordinate lines:

$$\cos\theta = \frac{1}{h_1 h_2} \left[\left(\frac{\partial \bar{y}}{\partial z}\right)_x \left(\frac{\partial \bar{y}}{\partial x}\right)_z + \left(\frac{\partial \bar{z}}{\partial x}\right)_z \left(\frac{\partial \bar{z}}{\partial z}\right)_x \right] \quad (3.3)$$

The geodesic curvature of the z =constant line

$$K_1 = \frac{1}{h_1^4 h_2 \sin\theta} \left\{ \left[\left(\frac{\partial \bar{y}}{\partial z}\right)_x \left(\frac{\partial \bar{z}}{\partial x}\right)_z - \left(\frac{\partial \bar{y}}{\partial x}\right)_z \left(\frac{\partial \bar{z}}{\partial z}\right)_x \right] \left[\left(\frac{\partial \bar{z}}{\partial x}\right) \frac{\partial^2 \bar{y}}{\partial x^2} - \frac{\partial \bar{y}}{\partial x} \frac{\partial^2 \bar{z}}{\partial x^2} \right]_z \right. \\ \left. + \left[\left(\frac{\partial \bar{y}}{\partial z}\right)_x \left(\frac{\partial^2 \bar{y}}{\partial x^2}\right)_z + \left(\frac{\partial \bar{z}}{\partial z}\right)_x \left(\frac{\partial^2 \bar{z}}{\partial x^2}\right)_z \right] \right\} \quad (3.4)$$

The geodesic curvature of the x =constant line

$$K_2 = \frac{-1}{h_1 h_2^4 \sin\theta} \left[\left(\frac{\partial \bar{y}}{\partial z}\right)_x \left(\frac{\partial \bar{z}}{\partial x}\right)_z - \left(\frac{\partial \bar{y}}{\partial x}\right)_z \left(\frac{\partial \bar{z}}{\partial z}\right)_x \right] \left[\left(\frac{\partial \bar{z}}{\partial z}\right) \frac{\partial^2 \bar{y}}{\partial z^2} - \frac{\partial \bar{y}}{\partial z} \frac{\partial^2 \bar{z}}{\partial z^2} \right]_x \quad (3.5)$$

The other parameters K_{12} and K_{21} are calculated from (2.6). It may be noted that K_1 and K_2 can also be obtained from (2.5). This provides a check on the expressions given by (3.4) and (3.5).

In boundary-layer calculations, we need the inviscid velocity components along the surface coordinates. Let \vec{V} be the total velocity vector on the hull, $(\bar{u}, \bar{v}, \bar{w})$ the corresponding velocity components in the Cartesian coordinates, and (u_e, w_e) in the adopted surface coordinates. As can be seen from figure 3,

$$u_e = \frac{\vec{V} \cdot \vec{t}_1 - \cos\theta \vec{V} \cdot \vec{t}_2}{\sin^2\theta} \quad (3.6)$$

$$w_e = \frac{\vec{V} \cdot \vec{t}_2 - \vec{V} \cdot \vec{t}_1 \cos \theta}{\sin^2 \theta} \quad (3.7)$$

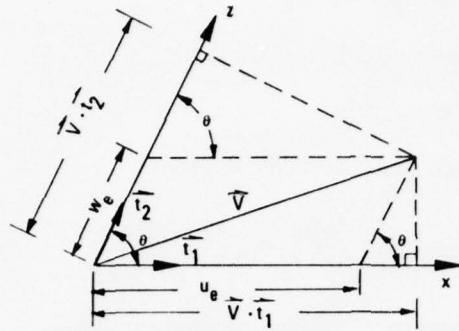


Figure 3. Resolution of the velocity components.

Here \vec{t}_1 and \vec{t}_2 are the unit tangent vectors along x and z coordinates and are given by

$$\vec{t}_1 = \frac{1}{h_1} \left[\vec{i} + \left(\frac{\partial \bar{y}}{\partial x} \right)_z \vec{j} + \left(\frac{\partial \bar{z}}{\partial x} \right)_z \vec{k} \right] \quad (3.8)$$

$$\vec{t}_2 = \frac{1}{h_2} \left[\left(\frac{\partial \bar{y}}{\partial z} \right)_x \vec{j} + \left(\frac{\partial \bar{z}}{\partial z} \right)_x \vec{k} \right] \quad (3.9)$$

With the definition of \vec{V} and with the use of (3.8) and (3.9), equations (3.6) and (3.7) can be written as

$$u_e = \frac{1}{\sin^2 \theta} \left\{ \left[\bar{u} + \bar{v} \left(\frac{\partial \bar{y}}{\partial x} \right)_z + \bar{w} \left(\frac{\partial \bar{z}}{\partial x} \right)_z \right] \frac{1}{h_1} - \frac{\cos \theta}{h_2} \left[\bar{v} \left(\frac{\partial \bar{y}}{\partial z} \right)_x + \bar{w} \left(\frac{\partial \bar{z}}{\partial z} \right)_x \right] \right\} \quad (3.10)$$

$$w_e = \frac{1}{\sin^2 \theta} \left\{ \frac{1}{h_2} \left[\bar{v} \left(\frac{\partial \bar{y}}{\partial z} \right)_x + \bar{w} \left(\frac{\partial \bar{z}}{\partial z} \right)_x \right] - \frac{\cos \theta}{h_1} \left[\bar{u} + \bar{v} \left(\frac{\partial \bar{y}}{\partial x} \right)_z + \bar{w} \left(\frac{\partial \bar{z}}{\partial x} \right)_z \right] \right\} \quad (3.11)$$

IV. NUMERICAL METHOD

We use the Box method to solve the boundary-layer equations given in Section II. This is a two-point finite-difference method developed by Keller and Cebeci. This method has been applied to two-dimensional flows as well as three-dimensional flows and has been found to be efficient and accurate. Descriptions of this method have been presented in a series of papers and reports and a detailed presentation is contained in a recent book by Cebeci and Bradshaw¹³.

In using this numerical method, or any other method, care must be taken in obtaining solutions of the equations when the transverse velocity component w contains regions of flow reversal. Such change in w -profiles will lead to numerical instabilities resulting from integration opposed to the flow direction unless appropriate changes are made in the integration procedure. Here we use the procedure developed by Cebeci and Stewartson. In this new and very powerful procedure, which follows the characteristics of the locally plane flow, the direction of w at each grid point across the boundary layer is checked and difference equations are written accordingly. At each point to be calculated, the backward characteristics which determine the domain of dependence, are computed from the local values of the velocity. Since the characteristic must be determined as part of the solution, in the calculation procedure a Newton iteration process is used to correctly determine the exact shape of the domain of dependence.

To illustrate the basic numerical method, we shall at first consider the solution of the longitudinal attachment-line equations (2.30) and (2.31) and then the solution of the full three-dimensional flow equations are given by (2.24) and (2.25). We shall not discuss the Cebeci-Stewartson procedure for computing three-dimensional flows with the transverse velocity, w , containing flow reversal since that procedure will be fully described in a forthcoming paper.

4.1 Difference Equations for the Longitudinal Attachment-Line Equations

According to the Box method, we first reduce the equations (2.30), (2.31), (2.32) and (2.26) into a system of five first-order equations by introducing new dependent variables $u(x,z,n)$, $v(x,z,n)$, $w(x,z,n)$, $t(x,z,n)$ and $\theta(x,z,n)$. Equations (2.30) and (2.31) can then be written as

$$u' = v \quad (4.1a)$$

$$w' = t \quad (4.1b)$$

$$(bv)' + \theta v - m_2 u^2 + m_{11} = m_{10} u \frac{\partial u}{\partial x} \quad (4.1c)$$

$$(bt)' + \theta t - m_4 uw - m_3 w^2 - m_9 u^2 + m_{12} = m_{10} u \frac{\partial w}{\partial x} \quad (4.1d)$$

$$\theta' = m_7 u + m_6 w + m_{10} \frac{\partial u}{\partial x} \quad (4.1e)$$

The boundary conditions (26) and (32) become

$$\eta = 0: \quad u = w = \theta = 0 \quad (4.2)$$

$$\eta = \eta_\infty: \quad u = 1, \quad w = w_{ze}/u_{ref}$$

We next consider the net rectangle shown in figure 4 and denote the net points by

$$\begin{aligned} x_0 = 0 & & x_n = x_{n-1} + k_n & & n = 1, 2, \dots, N \\ \eta_0 = 0 & & \eta_j = \eta_{j-1} + h_j & & j = 1, 2, \dots, J \end{aligned}$$

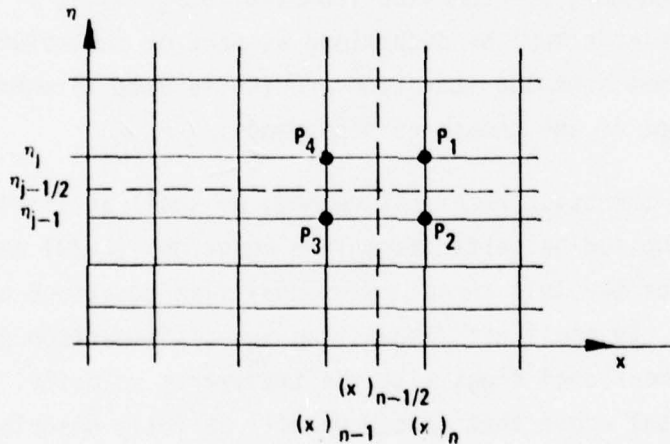


Figure 4. Net rectangle for the longitudinal attachment-line equations.

We approximate the quantities (u, v, g, t, θ) at points (x_n, η_j) of the net by functions denoted by $(u_j^n, v_j^n, w_j^n, t_j^n, \theta_j^n)$. We also employ the notation for points and quantities midway between net points and for any net function s_j^n :

$$\begin{aligned}
x_{n-1/2} &= \frac{1}{2} [x_n + x_{n-1}] & \eta_{j-1/2} &= \frac{1}{2} (\eta_j + \eta_{j-1}) \\
s_j^{n-1/2} &= \frac{1}{2} (s_j^n + s_j^{n-1}) & s_{j-1/2} &= \frac{1}{2} (s_j^n + s_{j-1}^n)
\end{aligned} \tag{4.3}$$

The difference equations which are to approximate (4.1) are formulated by considering one mesh rectangle as in figure 4. We approximate (4.1a,b) using centered difference quotients and average them about the midpoint $(x_n, \eta_{j-1/2})$ of the segment P_1P_2 .

$$h_j^{-1} (u_j^n - u_{j-1}^n) = v_{j-1/2}^n \tag{4.4a}$$

$$h_j^{-1} (w_j^n - w_{j-1}^n) = t_{j-1/2}^n \tag{4.4b}$$

Similarly, (4.1c,d,e) are approximated by centering them about the midpoint $(x_{n-1/2}, \eta_{j-1/2})$ of the rectangle $P_1P_2P_3P_4$. This gives

$$h_j^{-1} [(bv)_j^n - (bv)_{j-1}^n] + (\theta v)_{j-1/2}^n - (m_2^n + \alpha_n)(u^2)_{j-1/2}^n = R_{j-1/2}^{n-1} - m_{11}^n \tag{4.4c}$$

$$\begin{aligned}
h_j^{-1} [(bt)_j^n - (bt)_{j-1}^n] + (\theta t)_{j-1/2}^n - (m_4^n + \alpha_n)(uw)_{j-1/2}^n - m_3^n (w^2)_{j-1/2}^n \\
- m_9^n (u^2)_{j-1/2}^n + \alpha_n [w_{j-1/2}^{n-1} u_{j-1/2}^n - u_{j-1/2}^{n-1} w_{j-1/2}^n] = S_{j-1/2}^{n-1} - m_{12}^n
\end{aligned} \tag{4.4d}$$

$$h_j^{-1} (\theta_j^n - \theta_{j-1}^n) - (m_1^n + 2\alpha_n)u_{j-1/2}^n - m_6^n w_{j-1/2}^n = T_{j-1/2}^{n-1} \tag{4.4e}$$

Here

$$\begin{aligned}
R_{j-1/2}^{n-1} = -\alpha_n (u^2)_{j-1/2}^{n-1} - \left\{ h_j^{-1} [(bv)_j^{n-1} - (bv)_{j-1}^{n-1}] + (\theta v)_{j-1/2}^{n-1} \right. \\
\left. - m_2^{n-1} (u^2)_{j-1/2}^{n-1} + m_{11}^{n-1} \right\}
\end{aligned} \tag{4.5a}$$

$$\begin{aligned}
S_{j-1/2}^{n-1} = -\alpha_n (uw)_{j-1/2}^{n-1} - \left\{ h_j^{-1} [(bt)_j^{n-1} - (bt)_{j-1}^{n-1}] + (\theta t)_{j-1/2}^{n-1} - m_{12}^{n-1} - m_4^{n-1} (uw)_{j-1/2}^{n-1} \right. \\
\left. - m_3^{n-1} (w^2)_{j-1/2}^{n-1} - m_9^{n-1} (u^2)_{j-1/2}^{n-1} \right\}
\end{aligned} \tag{4.5b}$$

$$T_{j-1/2}^{n-1} = -2\alpha_n u_{j-1/2}^{n-1} - \left\{ h_j^{-1} (\theta_j^{n-1} - \theta_{j-1}^{n-1}) - m_1^{n-1} u_{j-1/2}^{n-1} - m_6^{n-1} w_{j-1/2}^{n-1} \right\} \quad (4.5c)$$

$$\alpha_n = \frac{m_{10}^{n-1/2}}{x_n - x_{n-1}} \quad (4.5d)$$

4.2 Difference Equations for the Full Three-Dimensional Equations

The difference equations for the full three-dimensional equations, as given by (2.24) and (2.25), are again expressed in terms of a first-order system. With the definitions given by (4.1a) and (4.1b), they are written as

$$(bv)' + \theta v - m_2 u^2 - m_5 uv - m_8 w^2 + m_{11} = m_{10} u \frac{\partial u}{\partial x} + m_7 w \frac{\partial u}{\partial z} \quad (4.6a)$$

$$(bt)' + \theta t - m_4 uw - m_3 w^2 - m_9 u^2 + m_{12} = m_{10} u \frac{\partial w}{\partial x} + m_7 w \frac{\partial w}{\partial z} \quad (4.6b)$$

$$\theta' = m_1 u + m_6 w + m_{10} \frac{\partial u}{\partial x} + m_7 \frac{\partial w}{\partial z} \quad (4.6c)$$

Their boundary conditions, (2.26) become:

$$\eta = 0: \quad u = w = \theta = 0 \quad (4.7a)$$

$$\eta = \eta_\infty: \quad u = 1, \quad w = w_e / u_{\text{ref}} \quad (4.7b)$$

The difference equations for (4.1a) and (4.1b) are the same as those given by (4.4a) and (4.4b): they are written for the midpoint $(x_n, z_i, \eta_{j-1/2})$ of the net cube shown in figure 5; that is

$$h_j^{-1} (u_j^{n,i} - u_{j-1}^{n,i}) = v_{j-1/2}^{n,i}, \quad h_j^{-1} (w_j^{n,i} - w_{j-1}^{n,i}) = t_{j-1/2}^{n,i} \quad (4.8)$$

The difference equations which are to approximate (4.6a,b,c) are rather lengthy. To illustrate the difference equations for these three equations, we consider the following model equation

$$(bv)' + \theta v + m_{11} = m_{10} u \frac{\partial u}{\partial x} + m_7 w \frac{\partial u}{\partial z} \quad (4.9)$$

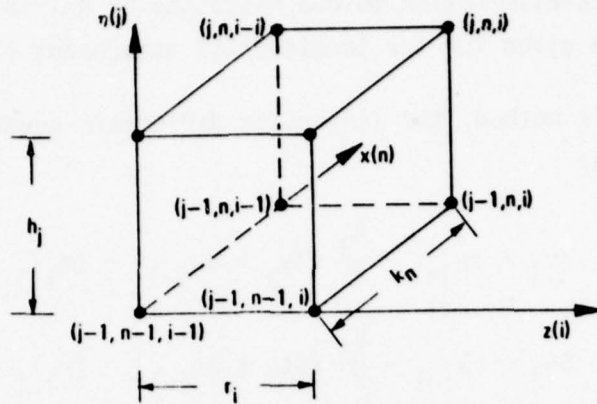


Figure 5. Net cube for the difference equations for three-dimensional flows, $w_j > 0$.

The difference equations for (4.9) are:

$$\begin{aligned}
 h_j^{-1} [(\bar{b}v)_j - (\bar{b}v)_{j-1}] + (\bar{v}v)_{j-1/2} + (m_{11})_{j-1/2}^{n-1/2} \\
 = (m_{10})_{i-1/2}^{n-1/2} \bar{u}_{j-1/2} \frac{\bar{u}_n - \bar{u}_{n-1}}{k_n} + (m_7)_{i-1/2}^{n-1/2} \bar{w}_{j-1/2} \frac{\bar{u}_i - \bar{u}_{i-1}}{r_i}
 \end{aligned} \quad (4.10)$$

Here, for example

$$\begin{aligned}
 \bar{v}_j &= \frac{1}{4} (v_j^{n,i} + v_j^{n,i-1} + v_j^{n-1,i-1} + v_j^{n-1,i}) \\
 \bar{u}_n &= \frac{1}{4} (u_j^{n,i} + u_j^{n,i-1} + u_{j-1}^{n,i} + u_{j-1}^{n,i-1}) \\
 \bar{u}_i &= \frac{1}{4} (u_j^{n,i} + u_j^{n-1,i} + u_{j-1}^{n,i} + u_{j-1}^{n-1,i})
 \end{aligned} \quad (4.11)$$

and

$$\begin{aligned}
 (m_{11})_{i-1/2}^{n-1/2} &= \frac{1}{4} [(m_{11})_i^n + (m_{11})_{i-1}^n + (m_{11})_i^{n-1} + (m_{11})_{i-1}^{n-1}] \\
 z_0 &= 0 \quad z_i = z_{i-1} + r_i \quad i = 1, 2, \dots, I
 \end{aligned} \quad (4.12)$$

4.3 Solution of the Difference Equations

The difference equations (4.4) for the longitudinal attachment-line flow and the difference equations for (4.6) are nonlinear algebraic equations. We use Newton's method to linearize them and then solve the resulting linear

system by the block-elimination method discussed by Keller¹⁴. A brief description of it will be given for the longitudinal attachment-line equations.

Using Newton's method, the linearized difference equations for the system given by (4.4) are:

$$\delta u_j - \delta u_{j-1} - \frac{h_j}{2} (\delta v_j + \delta v_{j-1}) = (r_1)_j \quad (4.13a)$$

$$\delta w_j - \delta w_{j-1} - \frac{h_j}{2} (\delta t_j + \delta t_{j-1}) = (r_2)_j \quad (4.13b)$$

$$\begin{aligned} (\zeta_1)_j \delta v_j + (\zeta_2)_j \delta v_{j-1} + (\zeta_3)_j \delta \theta_j + (\zeta_4)_j \delta \theta_{j-1} + (\zeta_5)_j \delta u_j \\ + (\zeta_6)_j \delta u_{j-1} = (r_3)_j \end{aligned} \quad (4.13c)$$

$$\begin{aligned} (\beta_1)_j \delta t_j + (\beta_2)_j \delta t_{j-1} + (\beta_3)_j \delta \theta_j + (\beta_4)_j \delta \theta_{j-1} + (\beta_5)_j \delta w_j \\ + (\beta_6)_j \delta w_{j-1} + (\beta_7)_j \delta u_j + (\beta_8)_j \delta u_{j-1} = (r_4)_j \end{aligned} \quad (4.13d)$$

$$\begin{aligned} (\sigma_1)_j \delta \theta_j + (\sigma_2)_j \delta \theta_{j-1} + (\sigma_3)_j \delta u_j + (\sigma_4)_j \delta u_{j-1} + (\sigma_5)_j \delta w_j \\ + (\sigma_6)_j \delta w_{j-1} = (r_5)_j \end{aligned} \quad (4.13e)$$

Here we have dropped the superscripts n, i and have defined $(r_k)_j$, $(\zeta_k)_j$, $(\beta_k)_j$ and $(\sigma_k)_j$ by

$$r_1 = u_{j-1} - u_j + h_j v_{j-1/2} \quad (4.14a)$$

$$r_2 = w_{j-1} - w_j + h_j t_{j-1/2} \quad (4.14b)$$

$$(r_3)_j = R_{j-1/2}^{n-1} - m_{11} - [(bv)_{j-1/2}' + (\theta v)_{j-1/2} - (m_2 + \alpha_n)(u^2)_{j-1/2}] \quad (4.14c)$$

$$\begin{aligned} (r_4)_j = S_{j-1/2}^{n-1} - m_{12} - [(bt)_{j-1/2}' + (\theta t)_{j-1/2} - (m_4 + \alpha_n)(uw)_{j-1/2} \\ - m_3(w^2)_{j-1/2} - m_9(u^2)_{j-1/2} + \alpha_n(w_{j-1/2}^{n-1} u_{j-1/2} - u_{j-1/2}^{n-1} w_{j-1/2})] \end{aligned} \quad (4.14d)$$

$$(r_5)_j = T_{j-1/2}^{n-1} - [\theta'_{j-1/2} - (m_1 + 2\alpha_n)u_{j-1/2} - m_6 w_{j-1/2}] \quad (4.14e)$$

$$(\zeta_1)_j = \frac{b_j}{h_j} + \frac{1}{2} \theta_j \quad (4.15a)$$

$$(\zeta_2)_j = -\frac{b_{j-1}}{h_j} + \frac{1}{2} \theta_{j-1} \quad (4.15b)$$

$$(\zeta_3)_j = \frac{1}{2} v_j \quad (4.15c)$$

$$(\zeta_4)_j = \frac{1}{2} v_{j-1} \quad (4.15d)$$

$$(\zeta_5)_j = -(m_2 + \alpha_n)u_j \quad (4.15e)$$

$$(\zeta_6)_j = -(m_2 + \alpha_n)u_{j-1} \quad (4.15f)$$

$$(\beta_1)_j = (\zeta_1)_j \quad (4.16a)$$

$$(\beta_2)_j = (\zeta_2)_j \quad (4.16b)$$

$$(\beta_3)_j = \frac{1}{2} t_j \quad (4.16c)$$

$$(\beta_4)_j = \frac{1}{2} t_{j-1} \quad (4.16d)$$

$$(\beta_5)_j = -\frac{1}{2} (m_4 + \alpha_n)u_j - m_3 w_j - \frac{1}{2} \alpha_n u_{j-1/2}^{n-1} \quad (4.16e)$$

$$(\beta_6)_j = -\frac{1}{2} (m_4 + \alpha_n)u_{j-1} - m_3 w_{j-1} - \frac{1}{2} \alpha_n u_{j-1/2}^{n-1} \quad (4.16f)$$

$$(\beta_7)_j = -\frac{1}{2} (m_4 + \alpha_n)w_j - m_9 u_j + \frac{1}{2} \alpha_n w_{j-1/2}^{n-1} \quad (4.16g)$$

$$(\beta_8)_j = -\frac{1}{2} (m_4 + \alpha_n)w_{j-1} - m_9 u_{j-1} + \frac{1}{2} \alpha_n w_{j-1/2}^{n-1} \quad (4.16h)$$

$$(\sigma_1)_j = \frac{1}{h_j} \quad (4.17a)$$

$$\xi = \begin{bmatrix} r_1 \\ r_2 \\ \xi_j \\ \xi_N \end{bmatrix} \quad \xi_j \equiv \begin{bmatrix} (r_1)_j \\ (r_2)_j \\ (r_3)_j \\ (r_4)_j \\ (r_5)_j \end{bmatrix} \quad \xi_j \equiv \begin{bmatrix} \delta u_j \\ \delta v_j \\ \delta w_j \\ \delta t_j \\ \delta \theta_j \end{bmatrix}$$

The A_j , B_j , C_j and A denote 5×5 matrices. The solution of (4.19) is obtained by the procedure described in Cebeci and Bradshaw¹³.

V. RESULTS

5.1 Turbulent Flow Calculations for a Curved Duct and Comparison with Experiment

The turbulence model described in Section II has been used with considerable success to compute a wide range of two-dimensional turbulent boundary layers, see for example Cebeci and Smith¹⁵. The model has also been used to compute three-dimensional flows and again is found to yield accurate results (see for example Cebeci^{9,10} and Cebeci, Kaups and Moser¹⁶). To further test the model for three-dimensional flows, we have considered the experimental data taken in a 60° curved duct of rectangular cross section. Figure 6 shows a sketch of the flow geometry. The experimental data are due to Vermeulen¹¹. Here z denotes the distance from the outer wall, measured along normals to the wall; x denotes the arc length along the outer wall; and y denotes distance normal to the plane x,z .

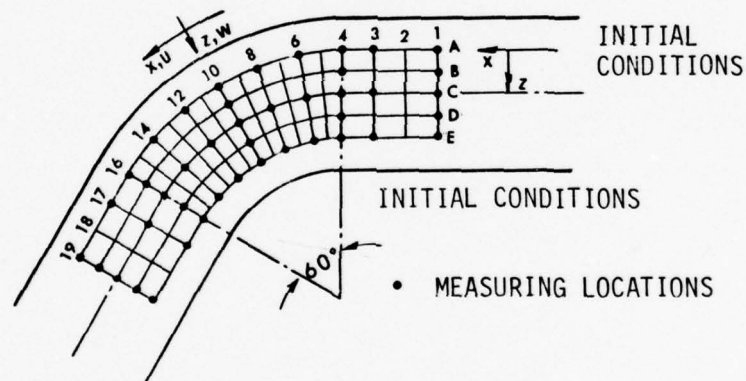


Figure 6. Coordinate system and notation for the curved duct.

To compare the computed results with the data, it is necessary to specify the initial profiles given by experiment. This can be done in a number of ways. In the study reported by Cebeci, Kaups and Moser¹⁶ the profiles were generated by using Coles' velocity profile formula. That formula, which represents the experimental data rather well for two-dimensional flows, was not very satisfactory for three-dimensional flows. Here we abandon the use of Coles' formula in favor of Thompson's two-parameter velocity profiles as described and improved by Galbraith and Head¹⁷. According to this formula,

the dimensionless u/u_e velocity profile is given by

$$\frac{u}{u_e} = \gamma_s \left(\frac{u}{u_e} \right)_{\text{inner}} + (1 - \gamma_s) \quad (5.1)$$

Here γ_s is an intermittency factor defined by the following empirical formulas:

$$\begin{aligned} 0 < \frac{y}{\delta_0} \leq 0.05 & \quad \gamma_s = 1 \\ 0.05 < \frac{y}{\delta_0} \leq 0.3 & \quad \gamma_s = 1 - 2.64214 \left(\frac{y}{\delta_0} - 0.05 \right)^2 \\ 0.3 < \frac{y}{\delta_0} \leq 0.7 & \quad \gamma_s = 4.4053 \left(\frac{y}{\delta_0} - 0.5 \right)^3 - 1.8502 \left(\frac{y}{\delta_0} - 0.5 \right) + 0.5 \\ 0.7 < \frac{y}{\delta_0} \leq 0.95 & \quad \gamma_s = 2.64214 \left(\frac{y}{\delta_0} - 0.05 \right)^2 \\ \frac{y}{\delta_0} > 0.95 & \quad \gamma_s = 0.0 \end{aligned} \quad (5.2)$$

The dimensionless velocity profile for the inner layer, that is, $(u/u_e)_{\text{inner}}$, is given by

$$\begin{aligned} y^+ < 4 & \quad u^+ = y^+ \\ 4 < y^+ < 30 & \quad u^+ = c_1 + c_2 \ln y^+ + c_3 (\ln y^+)^2 + c_4 (\ln y^+)^3 \\ y^+ > 30 & \quad u^+ = 5.50 \ln y^+ + 5.45 \end{aligned} \quad (5.3)$$

Here $c_1 = 4.187$, $c_2 = -5.745$, $c_3 = 5.110$, $c_4 = -0.767$, $y^+ = yu_\tau/\nu$, $u_\tau = (\tau_w/\rho)^{1/2}$, $u^+ = u/u_\tau$ and δ_0 is a parameter which is a function of θ , c_f and H .

To find the functional relationship between δ_0 , c_f , θ and H , we use the definitions of displacement thickness δ^* and momentum thickness θ . Substituting (5.1) into the definition of δ^* , after some algebra, we get

$$\frac{\delta^*}{\delta_0} \left(1 - \frac{A_1}{R_{\delta^*}} \right) = 0.5 + \sqrt{\frac{c_f}{2}} \left[A_4 \ln \frac{\delta^*}{\delta_0} - A_3 - A_2 \ln \left(R_{\delta^*} \sqrt{\frac{c_f}{2}} \right) \right] \quad (5.4)$$

where

$$A_1 = 50.679, \quad A_2 = 1.1942, \quad A_3 = 0.7943, \quad A_4 = 1.195$$

An expression similar to that given by (5.4) can also be obtained if we substitute (5.1) into the definition of θ . However, the resulting expression is quite complicated. For this reason, the expression for θ is obtained numerically, and for a given value of θ and H , the corresponding values of c_f and δ_0 are computed from that equation and from (5.4).

Equation (5.1) is recommended for two-dimensional flows. Here we assume that it also applies to the streamwise velocity profile by replacing u/u_e by u_s/u_{se} with c_f now representing the streamwise skin-friction coefficient.

In order to generate the crossflow velocity component (u_n/u_{se}), we use Mager's expression and define u_n/u_{se} by

$$\frac{u_n}{u_{se}} = \frac{u_s}{u_{se}} \left(1 - \frac{y}{\delta}\right)^2 \tan\beta_w \quad (5.5)$$

with the limiting crossflow angle β_w obtained from the experimental data.

Once the streamwise and crossflow velocity profiles are calculated by the above procedure, we compute the velocity profiles u/u_e and w/w_e in the orthogonal directions x and z by the following relationships

$$\frac{u}{u_e} = \frac{u_s}{u_{se}} - \frac{u_n}{u_{se}} \frac{w_e}{u_e} \quad (5.6a)$$

$$\frac{w}{w_e} = \frac{u_s}{u_{se}} + \frac{u_n}{u_{se}} \frac{u_e}{w_e} \quad (5.6b)$$

Figure 7 shows a comparison of generated and experimental total velocity profiles along the line A. As can be seen, the above discussed procedure for generating the initial velocity profiles from the experimental data is quite good. This is important for an accurate evaluation of a turbulent model especially for three-dimensional flows. Here

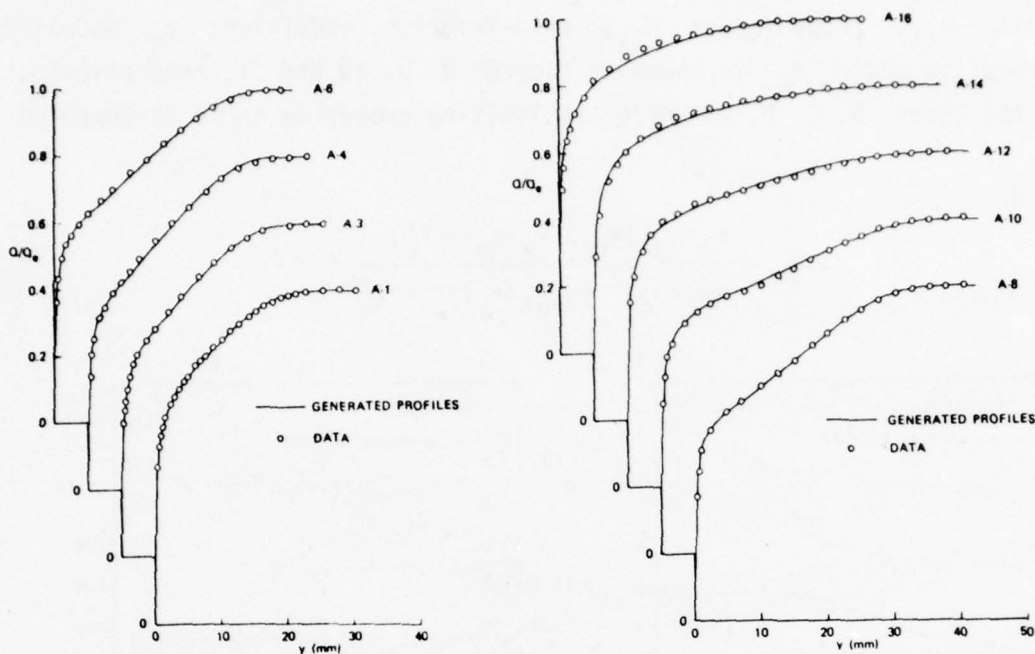


Figure 7. Comparison of generated initial total velocity profiles with Vermeulen's data.

$$\frac{Q}{Q_e} = \left(\frac{u^2 + w^2}{u_e^2 + w_e^2} \right)^{1/2} \quad (5.7)$$

The solution of the boundary-layer equations also requires the specification of the metric coefficients and the geodesic curvatures. They are calculated from the following expression:

$$h_1 = \begin{cases} 1 & \text{straight section} \\ 1 - z/R_0 & \text{curved section} \end{cases}$$

$$h_2 = 1.0, \quad K_2 = 0 \quad (5.8)$$

$$K_1 = \begin{cases} 0 & \text{straight section} \\ 1/(R_0 - z) & \text{curved section} \end{cases}$$

A comparison of calculated and experimental values of streamwise momentum thickness θ_{11} , shape factor H_{11} , skin-friction coefficient c_f and limiting crossflow angle β_w is shown in figures 8, 9, 10 and 11, respectively, along the lines B, C, D, E. Here the limiting crossflow angle is computed from

$$\tan\beta_w = \frac{w_e/u_e [(u_{ref}/u_e)g_w'' - f_w'']}{(w_e/u_e)^2 (u_{ref}/w_e)g_w'' + f_w''} \quad (5.9)$$

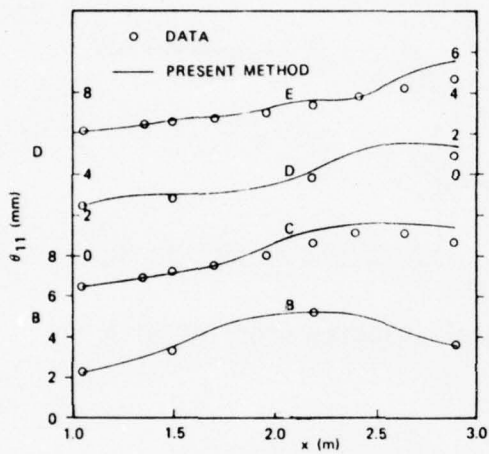


Figure 8. Comparison of computed momentum thickness with Vermeulen's data.

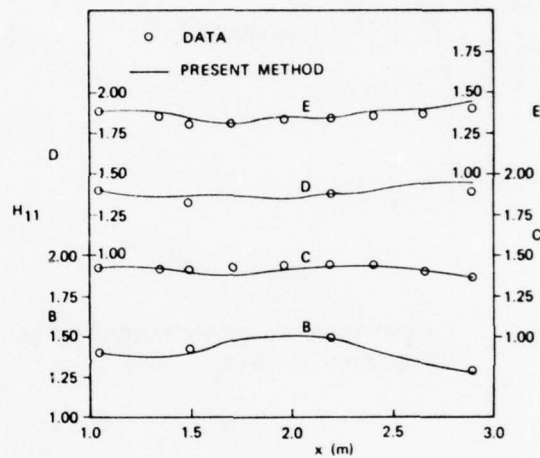


Figure 9. Comparison of computed shape factor with Vermeulen's data.

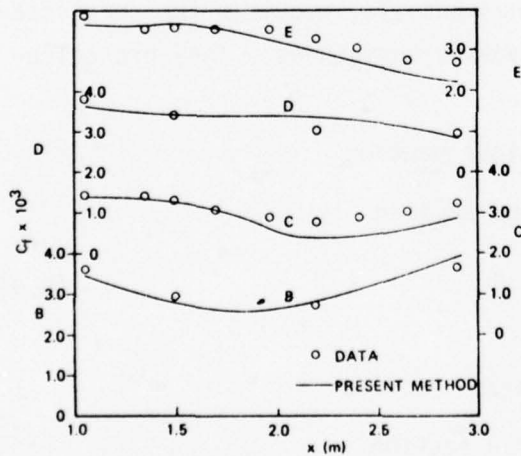


Figure 10. Comparison of computed skin friction coefficient with Vermeulen's data.

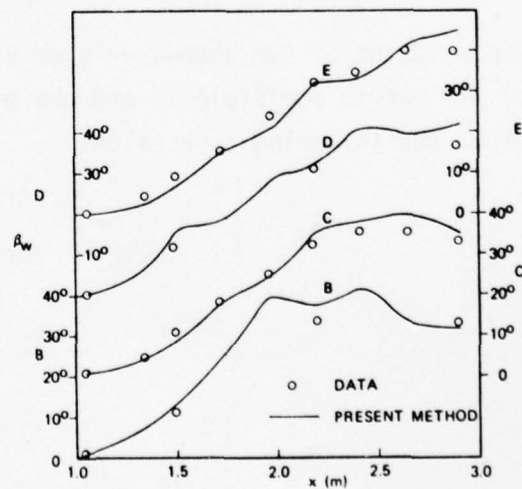


Figure 11. Comparison of computed limiting crossflow angle with Vermeulen's data.

Figures 12 and 13 show a comparison of calculated and experimental total velocity profiles and crossflow angle profiles along the lines C and E. Here the crossflow angle is computed from

$$\sin\beta = \frac{w_e/u_e [(u_{ref}/w_e)g' - f']}{Q/Q_e (Q_e/u_e)^2} \quad (5.10)$$

As in figures 8 through 11, again the agreement between calculated results and experiment is very good. The computed results follow the trend in the experimental data well and indicate that the present turbulence model, as in two-dimensional flows, is quite satisfactory for three-dimensional flows.

5.2 Results for a Double Elliptic Ship Model

To test our method for ship hulls, we have considered two separate hulls. The first one, which is discussed in this section, is a double elliptic ship whose hull is given analytically. The second one, which is discussed in section C, is ship model 5350 which has a rather complex shape. Its hull is represented section-by-section in tabular form and contains all the features of most merchant and naval vessels. It proves an excellent test case to study the computational difficulties associated with real ship hulls.

The double elliptic ship model can be analytically represented by

$$\bar{y} = f(\bar{x}, \bar{z}) = B \left[1 - \left(\frac{\bar{x}}{L} \right)^2 \right]^{1/2} \left[1 - \left(\frac{\bar{z}}{H} \right)^2 \right]^{1/2} \quad (5.11)$$

It has round edges except for the sharp corners at $\bar{x} = \pm L$ and $\bar{z} = \pm H$. The body of $L:H:B = 1.0:0.125:0.1$ together with the nonorthogonal coordinate nets on the hull is shown in figure 14.

The potential-flow solutions were obtained from the Douglas-Neumann computer program for three-dimensional flows. To get the solutions, 120 control elements on the surface were used, 12 along the \bar{x} -direction and 10 along the \bar{z} -direction.

Before we describe our boundary-layer calculations, it is useful to discuss the pressure distribution for this body shown in figure 15. As can be

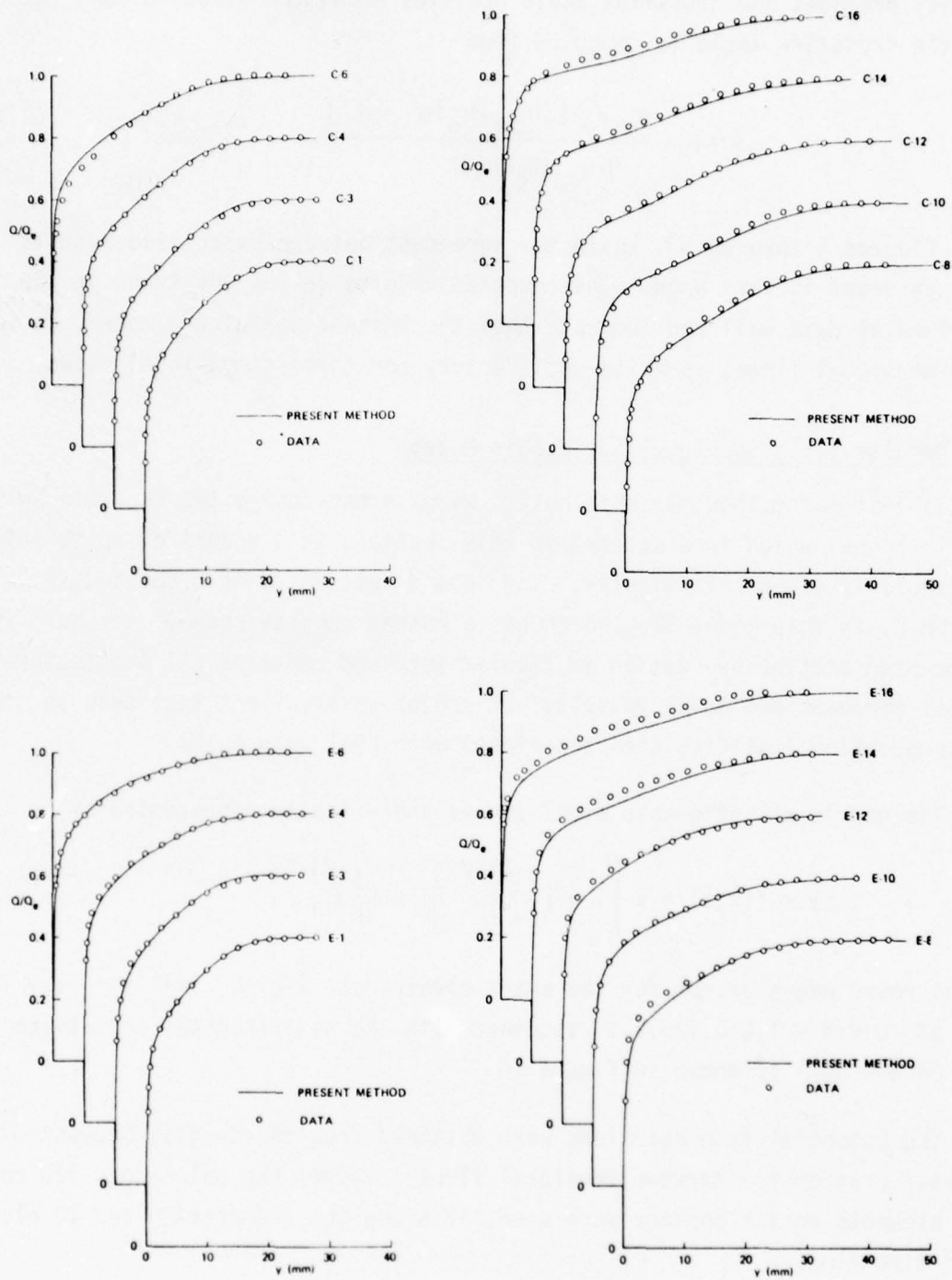


Figure 12. Comparison of computed total velocity profiles with Vermeulen's data.

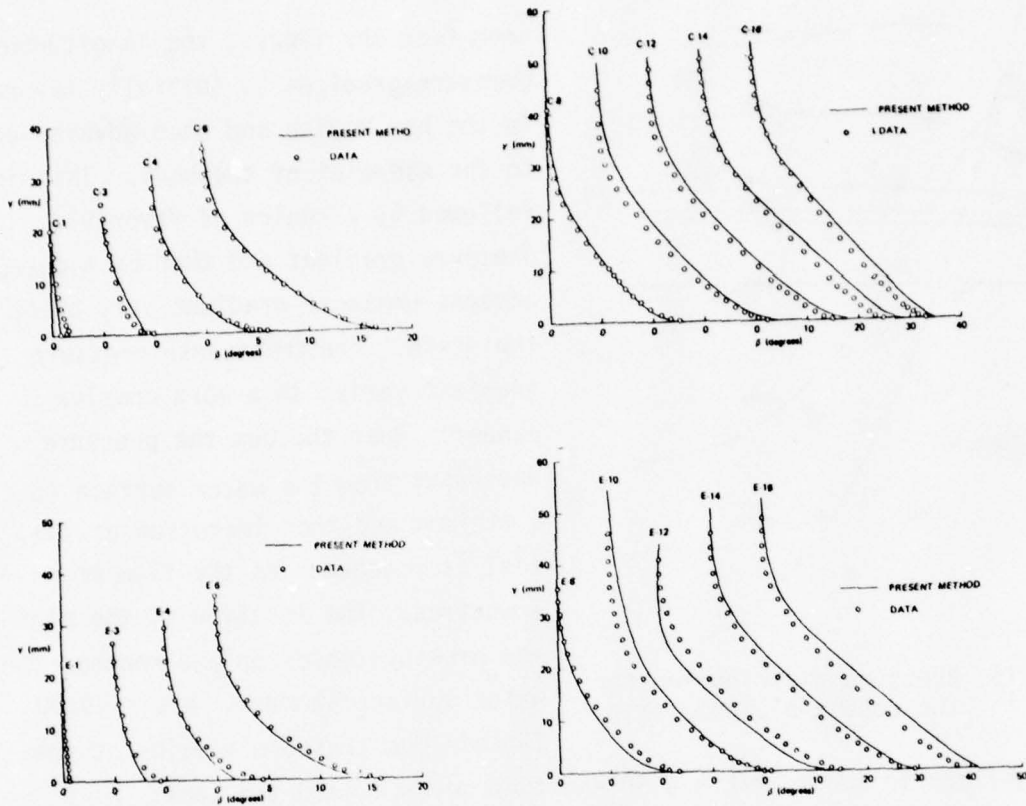


Figure 13. Comparison of computed crossflow angle with Vermeulen's data.



Figure 14. Three-dimensional picture of double elliptic ship model with the nonorthogonal coordinate system.

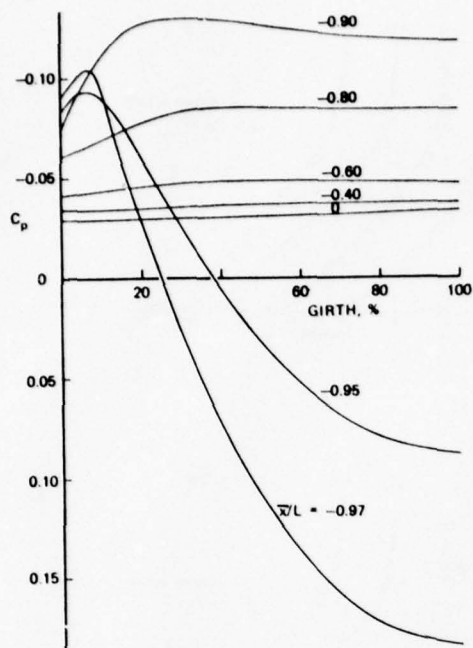


Figure 15. Pressure distribution for the double-elliptic ship.

seen from the figure, the longitudinal pressure gradient is initially favorable in the bow region and then adverse up to the midpoint of the body. This is followed by a region of favorable pressure gradient and then by a sharp adverse pressure gradient very close to the stern. The transverse pressure gradient varies in a more complex manner. Near the bow the pressure decreases from the water surface to a minimum and then increases as the keel is reached. As the flow moves downstream, the location of the minimum pressure moves up and reaches the water surface at about $x/L = -0.80$.

The minimum pressure remains at the water surface to about $x/L = 0.80$ and then moves toward the keel. As a result, near the bow and the stern, one may expect flow reversal of the transverse profiles while on the remaining major part of the ship hull, the transverse across the boundary layer does not reverse direction from the keel to the water surface. This conclusion is drawn from considering the pressure gradients only. The real situation may be somewhat modified because, in addition, there are the upstream effects and the curvature effects on the flow characteristics.

The boundary-layer computation starts with turbulent flow from $\bar{x}/L = -0.90$. We have tried to start the computation from $\bar{x}/L = -0.97$ and $\bar{x}/L = -0.95$. However, flow separation was observed at $\bar{x}/L = -0.90$ near the keel due to the sharp curvature and adverse pressure gradient in the bow region and can be seen from figure 15. In the previous calculations of Chang and Patel⁶ and Cebeci and Chang⁷, the flow separation near the bow was not found due to the orthogonal coordinate system they adopted in which the second net point from the keel is so far from the keel that the region of adverse pressure gradient is omitted.

In our boundary-layer calculations, we have used 40 points along the x-direction and 16 points along the z-direction. In the normal direction, we have taken approximately 40 points. The nonuniform grid structure described in Cebeci and Bradshaw¹³ is employed in the normal direction so that the grid points are concentrated near the wall where the velocity gradients are large.

Some of the computed results for $R_L = 10^7$ are shown in figures 16 to 18. Figure 16 shows the transverse distributions of the pressure coefficients, c_p , local skin-friction coefficient, c_f , the shape factor H_{11} , the Reynolds number based on the momentum thickness, R_θ and the limiting cross-flow angle for $x/L = -0.85, -0.50, 0.0, 0.25, 0.50, 0.75$. As can be seen from these figures, the boundary-layer parameters vary greatly near the keel where the curvatures and the pressure gradients are large and remain almost unchanged near the water surface where the curvatures and the pressure gradients are small. Except at $x/L = -0.85$, the limiting crossflow angle is positive. This implies that the crossflow near the wall moves from the keel to the free surface as predicted from the pressure distribution. Figure 17 shows typical longitudinal and transverse velocity profiles at $z = 0.6$ for several values

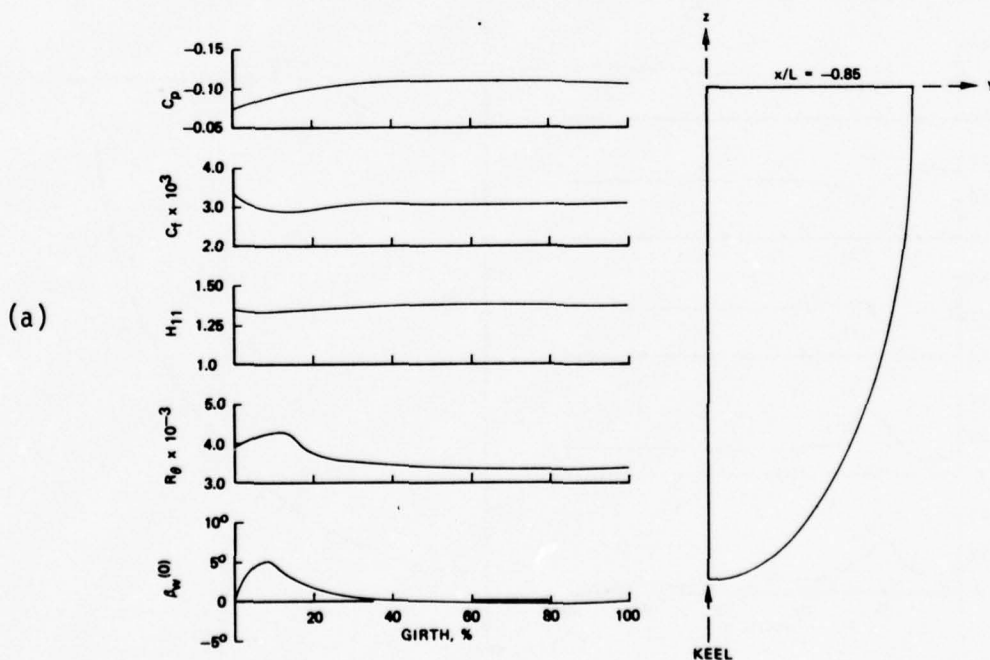


Figure 16. Computed c_p , c_f , H_{11} , R_θ and β_w for the double-elliptic ship model for $R_L = 10^7$ at (a) $x/L = -0.85$, (b) $x/L = -0.50$, (c) $x/L = 0.0$, (d) $x/L = 0.25$, (e) $x/L = 0.50$, (f) $x/L = 0.75$.

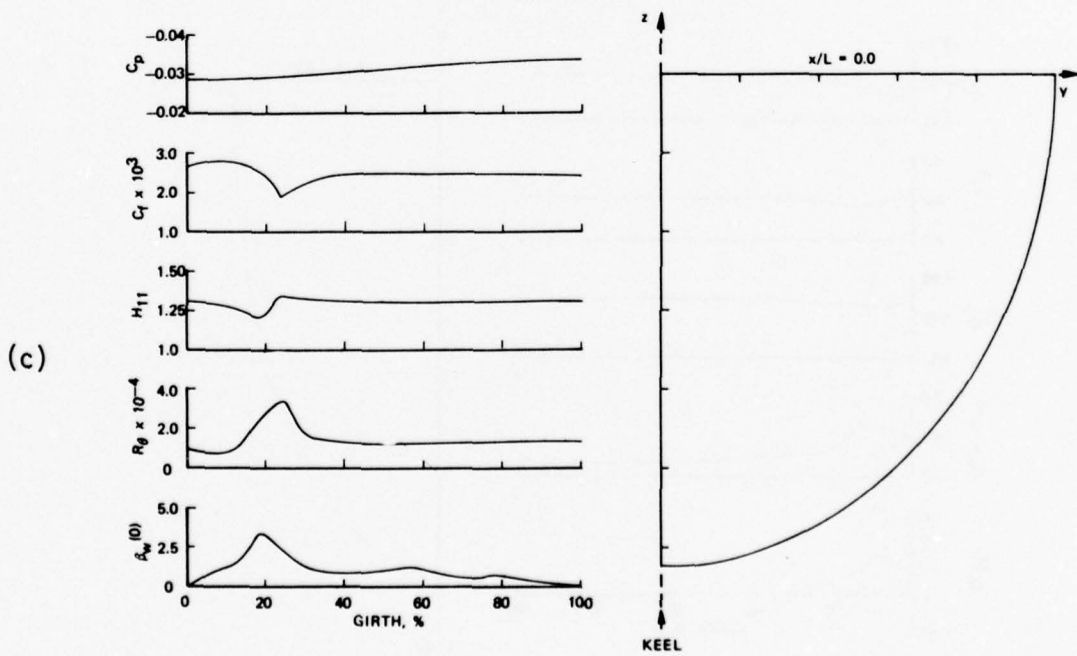
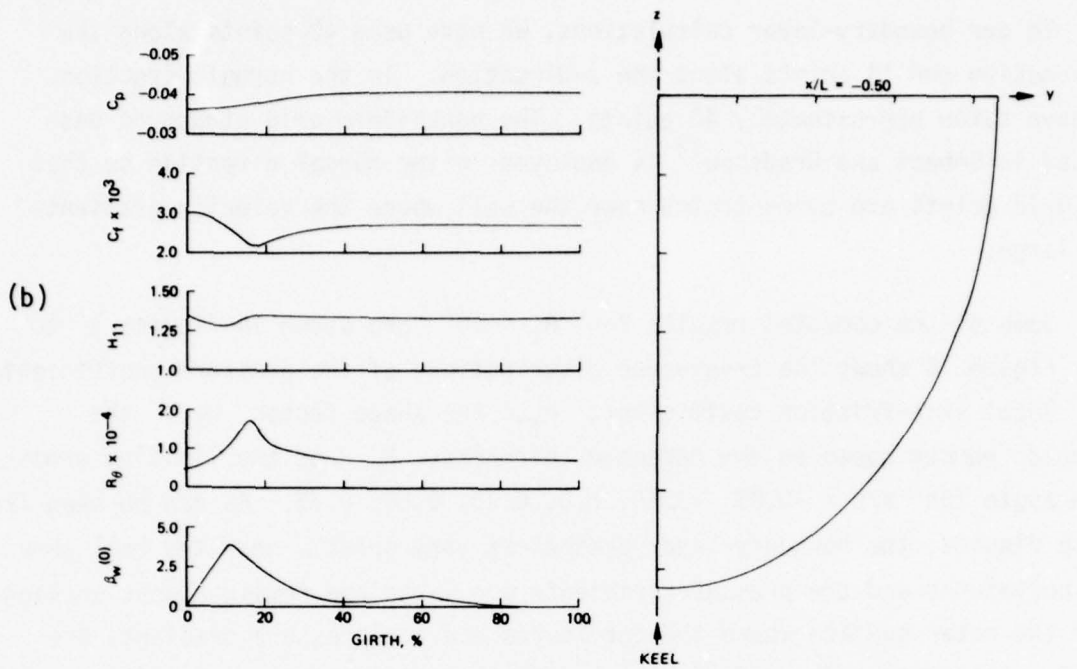


Figure 16. Continued.

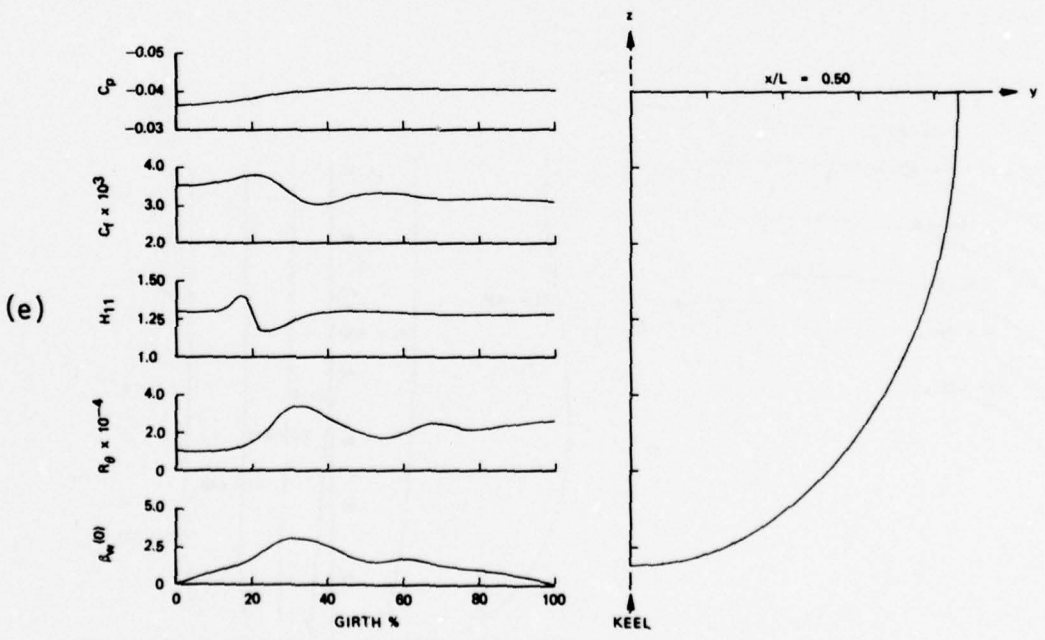
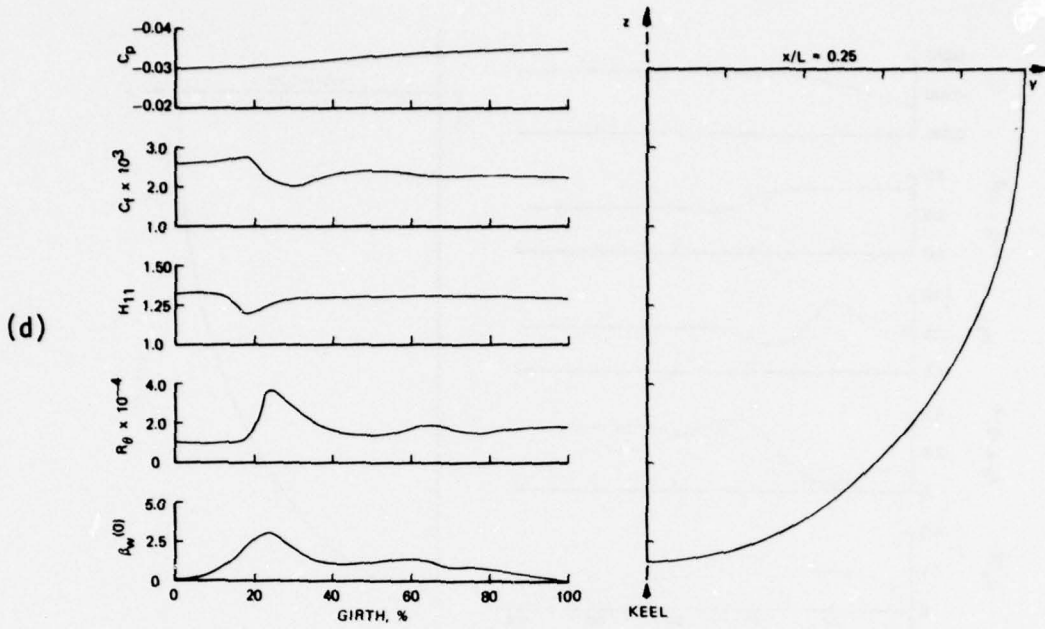


Figure 16. Continued.

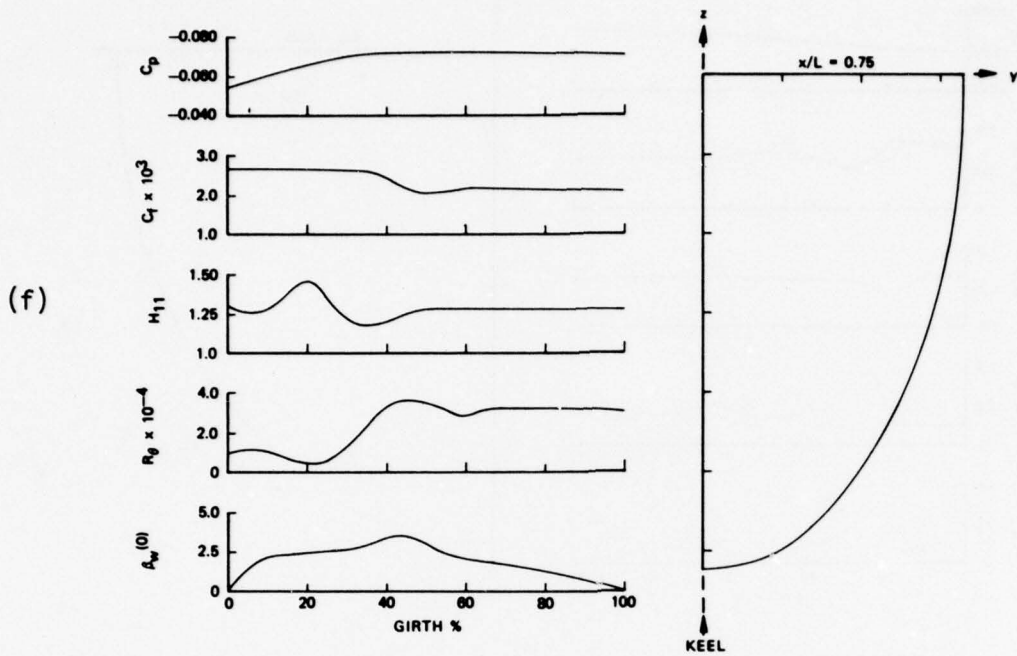


Figure 16. Continued.

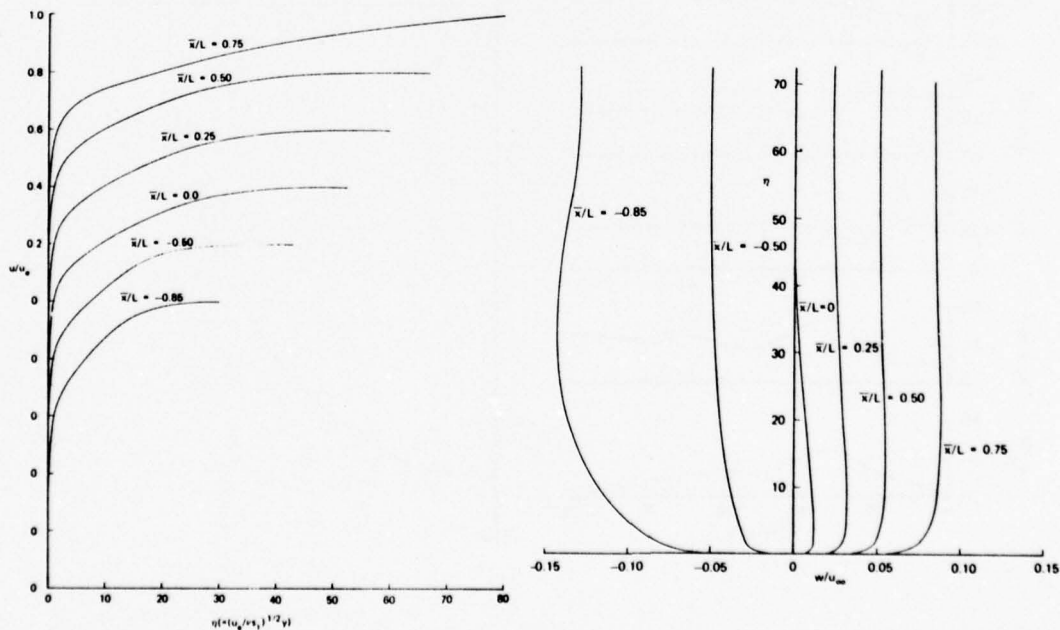


Figure 17. Computed longitudinal and transverse velocity profiles for the double-elliptic ship model for $R_L = 10^7$ at $z = 0.6$.

of x/L and figure 18 shows typical transverse velocity profiles at $x/L = -0.2$ for several values of z . As can be seen from figures 17(b) and 18, the transverse velocity component undergoes drastic changes in the longitudinal and transverse directions under the influence of pressure gradient and body geometry. As was discussed before, when the transverse velocity changes sign across the boundary layer and contains regions of reverse flow, numerical instabilities result from integration opposed to flow direction unless appropriate changes are made in the integration procedure. The new numerical procedure of Cebeci and Stewartson handles this situation very well and does not show any signs of breakdown resulting from flow reversal of transverse velocity component.

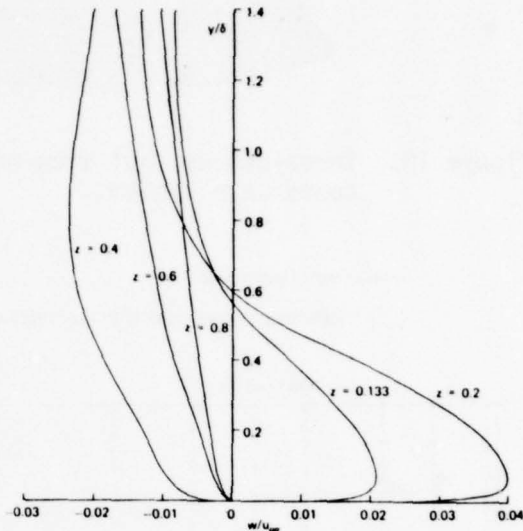


Figure 18. Computed transverse velocity profiles for the double-elliptic ship model at $x/L = -0.2$.

5.3 Results of Ship Model 5350

The ship model 5350, unlike the one discussed in section B, is a realistic tanker model. The geometry of the hull is so complicated that it is represented in tabular form section by section. The model possesses all the special features of existing merchant and naval vessels, that is, a bottom which is flat and not parallel to the still-water surface and an extended bow completely submerged under the water surface, and consequently serves as an excellent case on which to apply our method.

Figure 19 shows a three-dimensional picture of this ship model together with our nonorthogonal coordinate system. We see from this figure that, as a by-product of the mapping method discussed earlier, the $z=\text{const.}$ coordinate lines are concentrated in the bow and corner regions where the curvature is large. Figure 20 shows different cross-sections (indicated by solid lines) and interpolated values obtained by a cubic-spline method (indicated by circles) from which the geometric parameters are obtained.

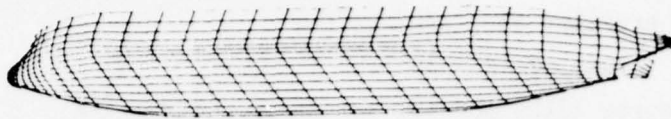


Figure 19. Three-dimensional view of ship model 5350 with the nonorthogonal coordinate system.

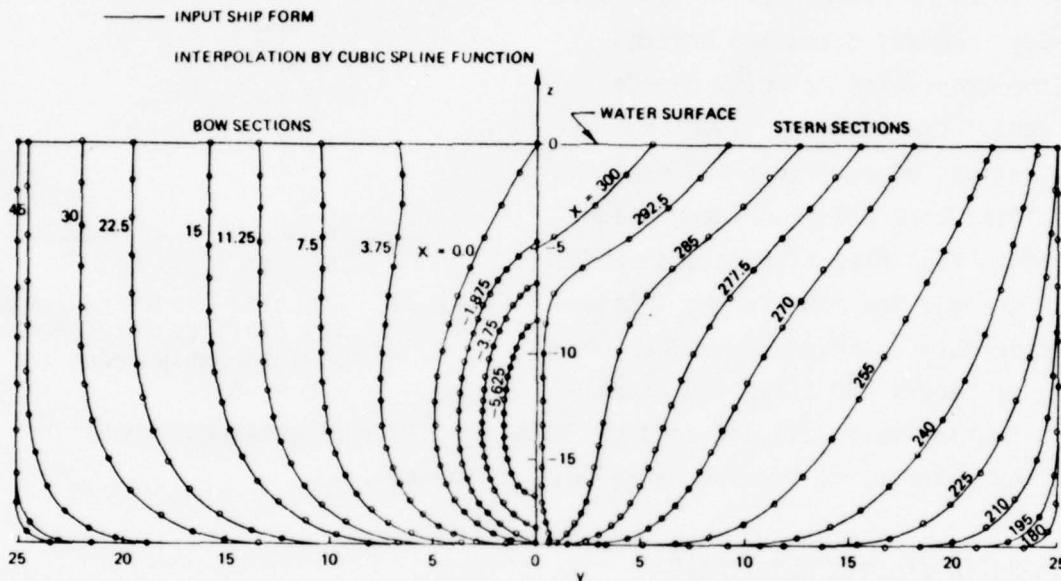


Figure 20. Body plan for ship model 5350.

The inviscid velocity distribution for the model is obtained by using the Douglas-Neumann method treating the model as a double ship model. Figure 21 shows the pressure distribution for the entire ship and figure 22 shows a detailed pressure distribution for the bow region. We see from these figures that the longitudinal pressure gradient near the keel is favorable and later becomes adverse. The pressure gradient in transverse direction decreases rapidly from the keel to a minimum value and then increases continuously up to the free surface. Due to this rapid pressure variation in the bow region, preliminary boundary-layer calculations showed flow separation and required an approximate procedure to generate the solutions for $x < 22.5\text{m}$. After that ($x > 22.5\text{m}$), the three-dimensional boundary-layer calculations were performed for a given inviscid pressure distribution. The initial conditions at $x = 22.5\text{m}$ were generated by solving the boundary-layer equations in which the z -wise

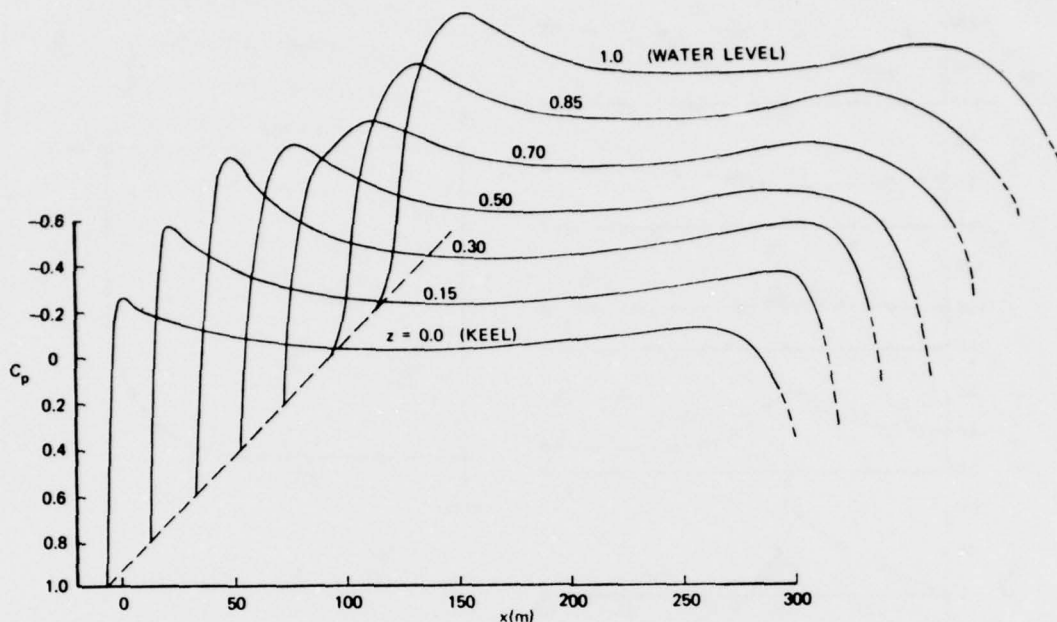


Figure 21. Pressure distribution for the entire ship model 5350.

derivatives for a constant z were neglected.

Figures 23 to 25 show some of the computed results for $R_L = 3 \times 10^8$. Figure 23 shows the variation of c_p , c_f , R_θ , H_{11} and β_w at the cross-planes of $x = 30m$, $60m$, $105m$, $165m$, $210m$. Typical streamwise velocity profiles at $x = 105m$ and $z = 0.2$ are shown in figure 24 and typical crossflow velocity profiles at $x = 60m$ are shown in figure 25. As can be seen from these figures, the crossflow velocity profiles show great variations and indicate clearly the flow reversal that takes place in the crossplanes. This implies that differential methods based on two-dimensional and/or small crossflow

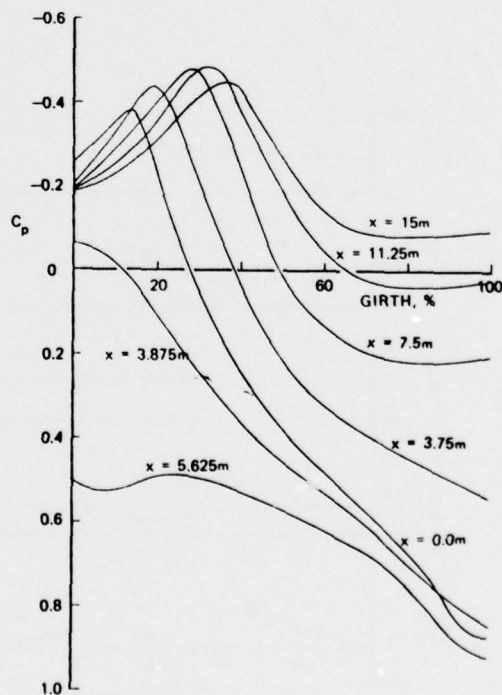


Figure 22. Pressure distribution for the bow region of ship model 5350.

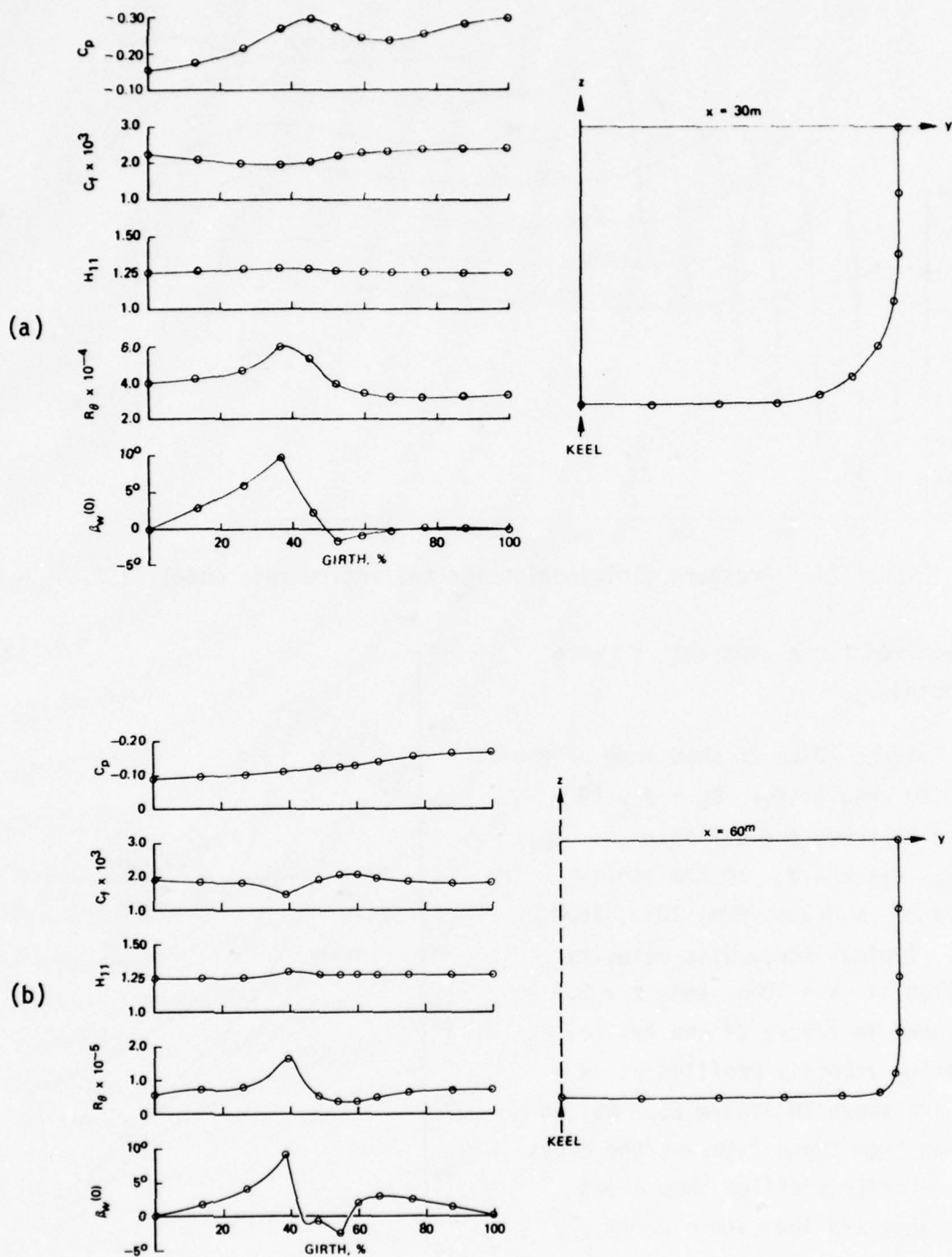


Figure 23. Computed c_p , c_f , H_{11} , R_θ and β_w for ship model 5350 for $R_L \approx 3 \times 10^8$ at (a) $x = 30m$, (b) $x = 60m$, (c) $x = 105m$, (d) $x = 165m$, (e) $x = 210m$.

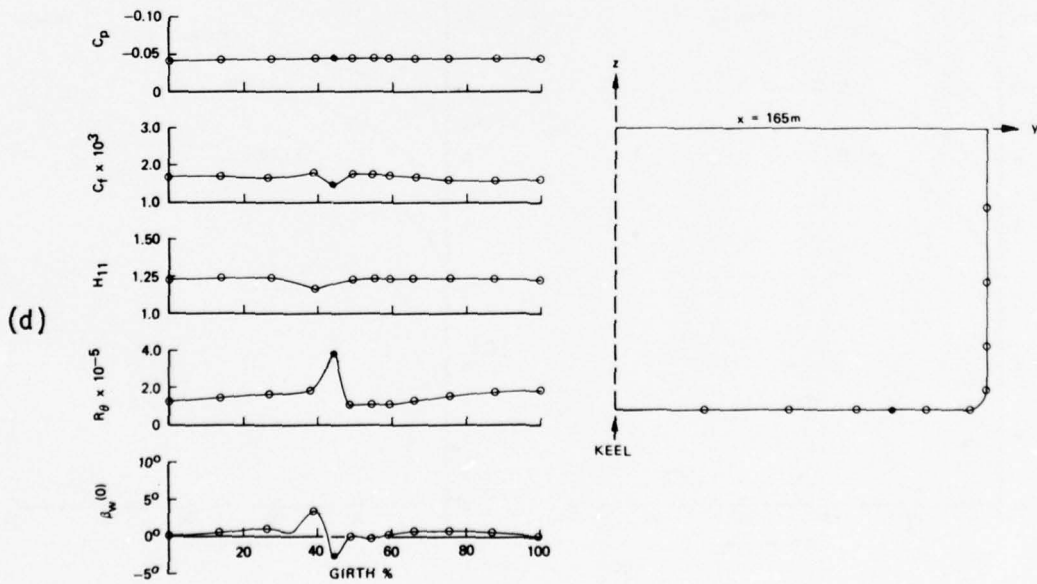
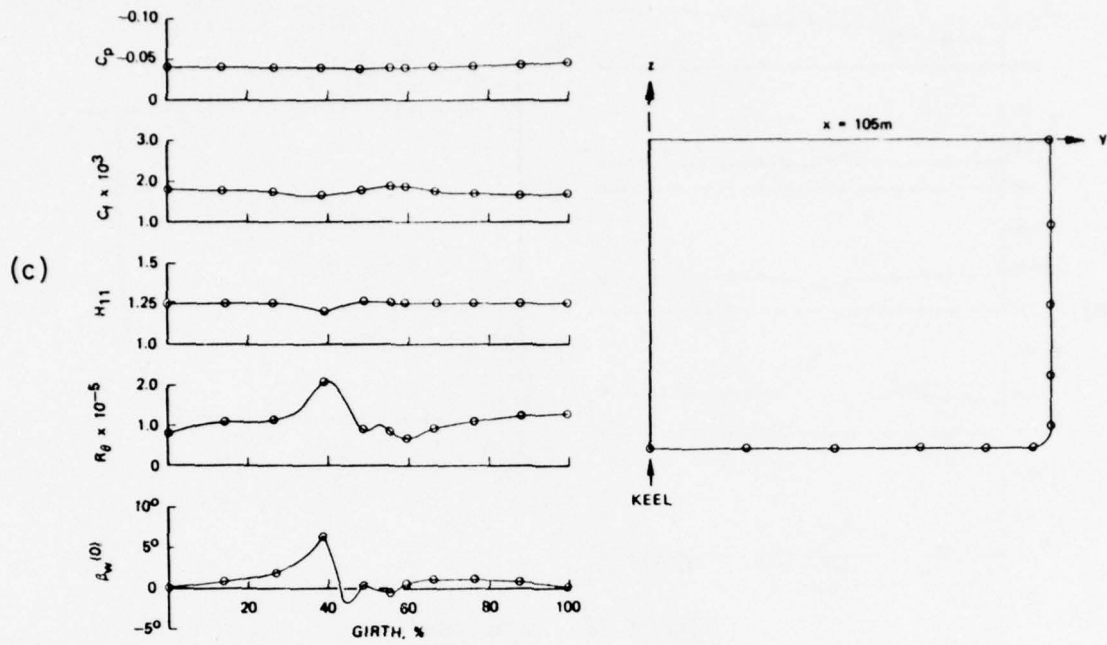


Figure 23. Continued.

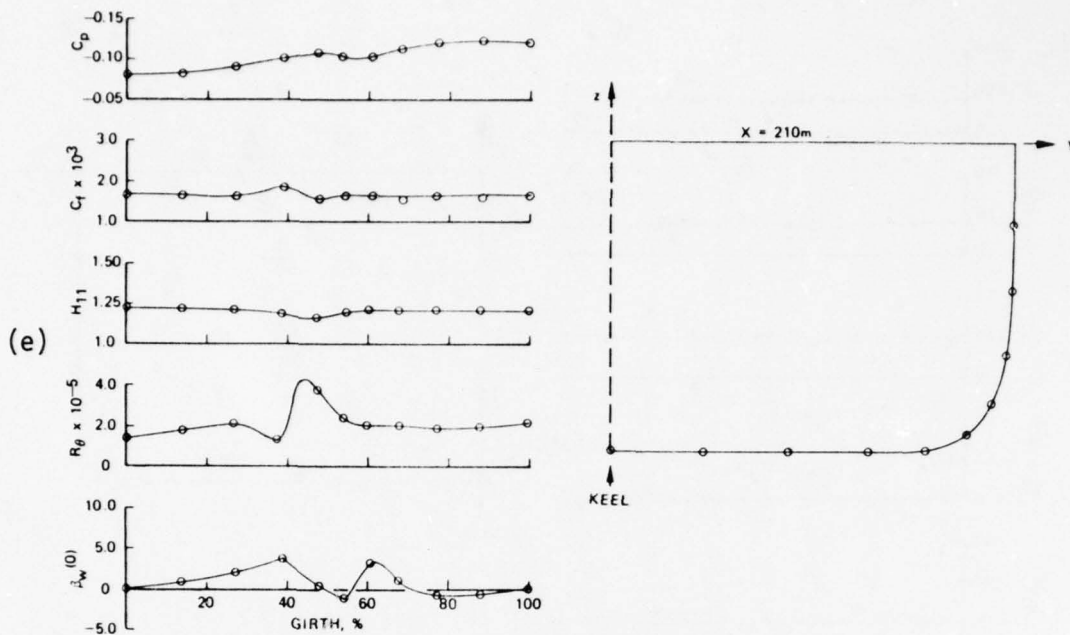


Figure 23. Continued

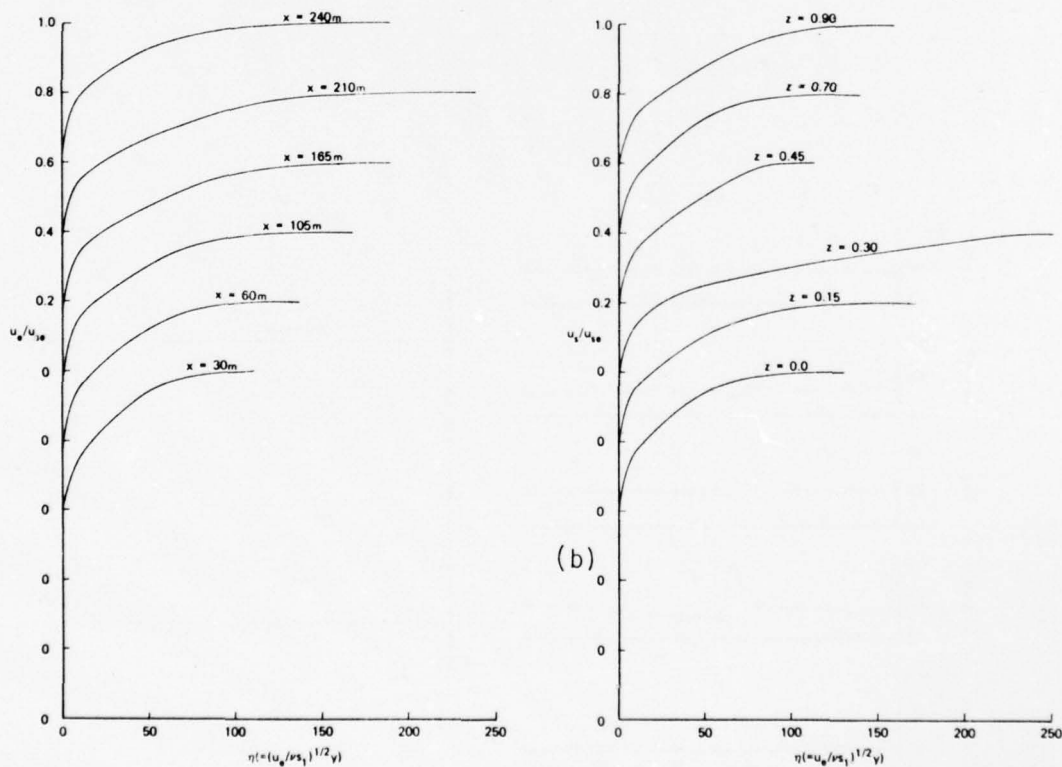


Figure 24. Computed streamwise velocity profiles for ship model 5350 for $Re = 3 \times 10^8$ along (a) $z = 0.2$ and (b) $x = 105m$ coordinate lines.

approximations as well as methods based on integral methods are not adequate to boundary-layer calculations on ship hulls. Other interesting results that emerge from these calculations are the sudden jumps of the limiting crossflow angle from positive to negative, and the thickening of the boundary layer in the corner region of the crossplanes. The jumps of the crossflow angle indicates the convergence of the flow from both sides of the corner region and, hence, enhances the thickening of the boundary layer. This thickening of the boundary layer in the corner region of ship hulls has been verified experimentally by Hoffman¹⁸.

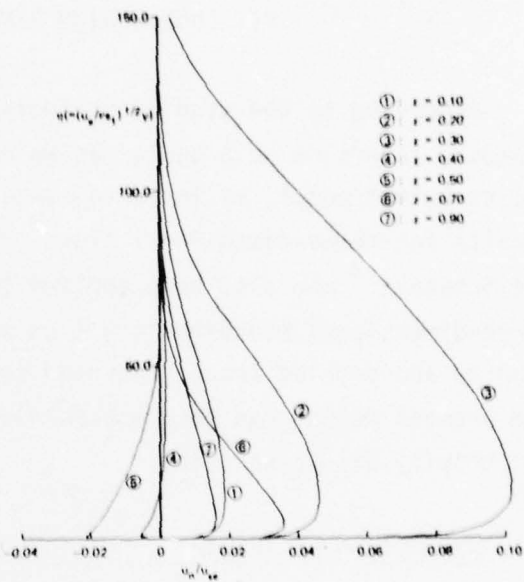


Figure 25. Computed crosswise velocity profiles for ship model 5350, for $R_L = 3 \times 10^8$ along $x = 60\text{m}$ coordinate line.

VI. CONCLUDING REMARKS AND FUTURE WORK

According to the studies presented in this paper, the three-dimensional boundary layers on ship hulls can be computed very efficiently and effectively. The turbulent model, as in two-dimensional flows, again yields satisfactory results for three-dimensional flows. This has been demonstrated by Soejima and Yamazaki¹⁹ who also have applied the present turbulence model to compute three-dimensional boundary layers on ship hulls. However, there are additional studies and problem areas that need to be considered and investigated before the present method can become a more effective tool to design ships. They are briefly discussed below.

6.1 Generation of Initial Conditions on Arbitrary Bow Configurations

In section 5-3, we presented calculations for the ship model 5350 and mentioned that due to flow separation in the bow region, we had to start the boundary-layer calculations at some distance away from the bow. Additional studies are required to generate the initial conditions on the bow. These studies can lead to a better design of bow configurations and to better handling of bilge vortices, which contribute to the total drag of the ship. However, this is by no means an easy task. Consider, for example, the ship model 5350 discussed earlier. A sketch of the bulbous nose with a plausible inviscid streamline distribution is shown in figure 26. We may assume that

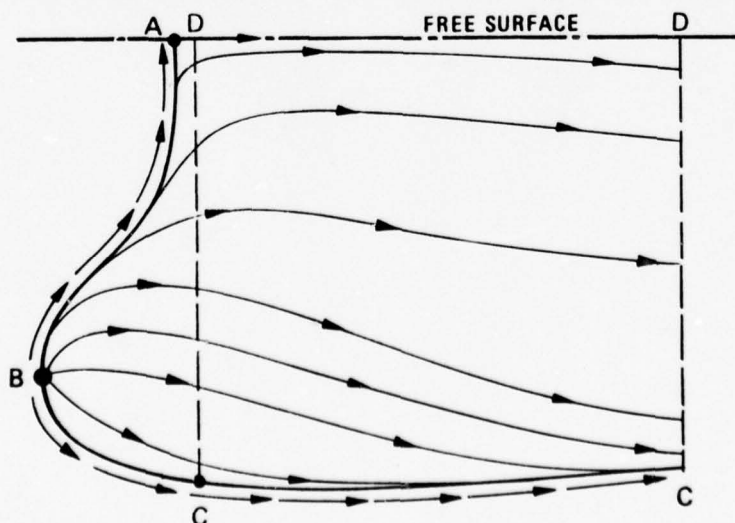


Figure 26. Pattern of streamlines near the bow of ship model 5350.

the ship is symmetrical about the keel plane and there is a nodal attachment point on the bulbous nose at B. If the ship is floating, then the water line is determined by conditions of constant pressure and zero normal velocity. Hence the intersection of the plane of symmetry with the water line at A is a saddle point with the streamlines of the inviscid flow converging on A along the line BA and diverging along an orthogonal direction. It is known that the boundary-layer equations can always be solved at B but that at A the situation is more complicated and furthermore it is still not entirely clear what their role is in relation to the general solution. It is likely, however, that provided no reversed flow occurs at A in the component of the solution along the direction BA, then separation can be avoided along this line by appropriate choice of design. Furthermore, if separation does occur, its effect may be limited. The recently developed Cebeci-Stewartson procedure however, can be applied to the present problem but there are some hurdles to be overcome.

Of particular difficulty is the choice of coordinate system on which to compute the solution and to join it with the already well-established method downstream of CD. We have seen that in the case of the prolate spheroid (see Cebeci, Khattab and Stewartson²⁰) it is helpful to have a mesh which is effectively Cartesian near the nose and the methods which were used to produce it in the earlier study are applicable to any body which can be represented by a paraboloid of revolution in the neighborhood of the nose. Now here we have a paraboloid near B but not one of revolution, but we believe that the necessary generalization is possible. The mesh now has to match with that which has proved convenient downstream of CD. Again we believe that a smooth transition can be achieved by building into the mesh sides, right from CBA, an appropriate spacing such that the points of a uniform mesh on CD are also points of this mesh although not, of course, at a constant value of one of the coordinates. Our evidence for this is based on a successful scheme that we have already worked out for the prolate spheroid, Cebeci, Khattab and Stewartson²⁰.

Other aspects that need further study include the condition at the water-line section. It has been usual to assume that the normal velocity is zero at the undisturbed free surface. This is not quite correct and the error may

have implications for the nature of the solution near A and especially the question of separation along BA. Even if separation does occur, it may be possible to handle the post-separation solution, since it probably extends only over a limited region of the ship, by means of an interaction theory, i.e. modifying the inviscid flow by means of a displacement surface.

6.2 Viscous-Inviscid Flow Interaction

The present boundary-layer calculations are done for a given pressure distribution obtained from an inviscid flow theory. In regions where the boundary-layer thickness is small, the inviscid pressure distribution does not differ much from the actual one; as a result, the boundary-layer calculations are satisfactory and agree well with experiment, see for example, the papers by Cebeci, Kaups and Moser¹⁶ and by Soejima and Yamazaki¹⁹. When the boundary-layer thickness is large, which is the case near the stern region, the effect of viscous flows on the inviscid pressure distribution must be taken into account. One possible way this can be done is to compute the displacement surface for a given inviscid pressure distribution and iterate. Such a procedure is absolutely necessary to account for the thickening of the boundary layer as was observed by Soejima and Yamazaki¹⁹.

6.3 Prediction of Wake Behind Ship Hulls

The present boundary-layer calculations can be done up to some distance close to the stern; after that, flow separation occurs. Since one, and probably the biggest, reason why there is interest in boundary-layer calculations on ship hulls, is the calculation of drag of the hull, additional studies should be directed to perform the calculations in the separated region and in the wake behind the ship. Recent calculation methods developed by Cebeci and his associates at Douglas for two-dimensional wake flows and for separated flows by using inverse boundary-layer theory are appropriate for these purposes.

VII. ACKNOWLEDGMENT

This work was supported by the David Taylor Naval Ship Research and Development Center under contract N00014-76-C-0950.

VIII. REFERENCES

1. Cebeci, T., Kaups, K. and Ramsey, J.A.: A General Method for Calculating Three-Dimensional Compressible Laminar and Turbulent Boundary Layers on Arbitrary Wings. NASA CR-2777, 1977.
2. Lin, J.D. and Hall, R.S.: A Study of the Flow Past a Shiplike Body. Univ. of Conn., Civil Engineering Department, Report No. CE66-7, 1966.
3. Miloh, T. and Patel, V.C.: Orthogonal Coordinate Systems for Three-Dimensional Boundary Layers with Particular Reference to Ship Forms. Iowa Institute of Hydraulic Research, Report No. 138, May 1972.
4. Keller, H.B.: A New Difference Scheme for Parabolic Problems. Numerical Solution of Partial Differential Equations, II, J. Bramble (ed.) Academic Press, New York, 1970.
5. Gadd, G.E.: The Approximate Calculation of Turbulent Boundary-Layer Development on Ship Hulls. RINA Paper W5, 1970.
6. Chang, K.C. and Patel, V.C.: Calculation of Three-Dimensional Boundary Layers on Ship Forms. Iowa Institute of Hydraulic Research, Report No. 176, 1975.
7. Cebeci, T. and Chang, K.C.: A General Method for Calculating Three-Dimensional Laminar and Turbulent Boundary Layers on Ship Hulls. 1. Coordinate System, Numerical Method and Preliminary Results. Report, Department of Mechanical Engineering, California State University at Long Beach, April 1977.
8. Rastogi, A.K and Rodi, W.: Calculation of General Three-Dimensional Turbulent Boundary Layers. AIAA Journal, Vol. 16, No. 2, pp 151-159, February 1978.
9. Cebeci, T.: Calculation of Three-Dimensional Boundary Layers, pt. 1, Swept Infinite Cylinders and Small Crossflow. AIAA Journal, Vol. 12, No. 6, pp. 779-786, June 1974.
10. Cebeci, T.: Calculation of Three-Dimensional Boundary Layers, pt. 2, Three-Dimensional Flows in Cartesian Coordinates. AIAA Journal, Vol. 13, No. 8, pp. 1056-1064, August 1975.
11. Vermulen, A.J.: Measurements of Three-Dimensional Turbulent Boundary Layers. Ph.D. Thesis, University of Cambridge, 1971.

12. Halsey, N.D.: Potential Flow Analysis of Multiple Bodies Using Conformal Mapping. M.S. Thesis, Department of Mechanical Engineering, California State University at Long Beach, 1977.
13. Cebeci, T. and Bradshaw, P.: Momentum Transfer in Boundary Layers, McGraw-Hill/Hemisphere Co., Washington, D.C., 1977.
14. Keller, H.B.: Accurate Difference Methods for Nonlinear Two-Point Boundary-Value Problems. SIAM J. Numerical Analysis, Vol. 11, No. 2, pp. 305-320, April 1974.
15. Cebeci, T. and Smith, A.M.O.: Analysis of Turbulent Boundary Layers, Academic Press, New York, 1974.
16. Cebeci, T., Kaups, K. and Moser, A.: Calculation of Three-Dimensional Boundary Layers, pt. 3, Three-Dimensional Incompressible Flows in Curvilinear Orthogonal Coordinates. AIAA Journal, Vol. 14, No. 8, pp. 1090-1094, August 1976.
17. Galbraith, R.A.McD., and Head, M.R.: Eddy Viscosity and Mixing-Length from Measured Boundary-Layer Developments. Aero Quarterly, XXVI, pp. 133-153, May 1975.
18. Hoffmann, H.P.: Untersuchung der 3-dimensionalen, turbulenten grenzschicht an einem schiffsdoppelmodell in wind kanal. Institut für Schiffbau der Universität, Hamburg, Bericht Nr. 343, 1976.
19. Soeijma, S. and Yamazaki, R.: Calculation of Three-Dimensional Boundary Layers on Ship Hull Forms. Trans West-Japan Soc. Naval Architects, No. 55, pp. 43-59, March 1978.
20. Cebeci, T., Khattab, A.A. and Stewartson, K.: Studies on Three-Dimensional Boundary Layers on Bodies of Revolution. Part 1. The Nose Separation. Douglas Aircraft Company Report, August 1978.

APPENDIX A
DESCRIPTION OF THE BOUNDARY-LAYER COMPUTER PROGRAM

This appendix describes in detail the computer program which calculates three-dimensional boundary layers on arbitrary ship hulls based on the non-orthogonal coordinate system and the numerical method described in the text. The computer program consists of two separate subprograms: the GEOMETRY and BOUNDARY-LAYER subprograms. The GEOMETRY subprogram requires the card input of the ship hull geometry section by section and the corresponding inviscid velocity components in a Cartesian coordinate system. It performs the following functions: (1) smooths the input data by the use of Fourier series expansion; (2) maps each section defining the ship hull onto a unit circle and defines the transverse stations, z , for boundary-layer calculations; (3) computes the geometric parameters, h_1 , h_2 , K_1 , K_2 , K_{12} , K_{21} , S_1 , and θ and the inviscid velocity components along the boundary-layer coordinate lines. In the steps 2 and 3, numerical interpolation and differentiation are frequently encountered. These operations are accomplished by the use of the cubic spline function. Because of the sensitivity of the spline function to smoothness of data, the input data (which are sections defining the ship hull and velocity components) have to be fairly smooth; if not, step 1, which is optional in the program, should be executed. Since the mapping of an arbitrary section onto a unit circle proceeds clockwise, it is convenient to use the right-handed Cartesian coordinate system for defining the ship hull. Hence, data defining each section must be input clockwise from the keel to the free surface.

The boundary-layer subprogram requires the geometric parameters, h_1 , etc., and the inviscid velocity distributions along the boundary-layer coordinate lines, which are the output of the geometry subprogram and are stored in tape unit 1. In addition, physical variables and program control parameters are input to indicate the unit Reynolds number, transition location, and specify the initial condition and to choose the grid points across the boundary layer. Details of the input instruction will be described later. The program logic and structure of the boundary-layer subprogram are rather complicated; the basic flow chart is shown in Figure A-1.

The computer program is written in Fortran IV for the IBM 370 system. When other systems are used to run the program, it is evident that slight modifications may be required to meet the specific requirements of that system. Three external units are used in the program for data storage. Unit 1 (defined as TAPEDT) is used in both the geometry and boundary-layer programs for storing the geometric parameters and freestream velocity distributions generated from the geometry program. Units 2 and 3 (defined as TAPEGP and TAPEPF) are exclusively used in the boundary-layer program as direct-access storage; unit 2 stores the body geometry and freestream velocity distributions; and unit 3 stores the pressure parameters and boundary-layer profiles. The region size needed to execute the program is about 200K bytes based on 41 longitudinal stations, 29 transverse stations and 61 grid points across the boundary layer.

The detailed input and output instructions of the program are provided below.

A-1 Input for the Geometry Program

Card 1 contains the title of the problem under consideration. The input is punched as 80-column alphanumeric field as shown below.

| | | | | | | | | | | | | | | | | | | | | | | | | | | | | | | | | | | | | | | | | | | | | | | | | | | | | | | | | | | | | | | | | | | | | | | | | | | | | | | | |
|-------|---|---|---|---|---|---|---|---|----|----|----|----|----|----|----|----|----|----|----|----|----|----|----|----|----|----|----|----|----|----|----|----|----|----|----|----|----|----|----|----|----|----|----|----|----|----|----|----|----|----|----|----|----|----|----|----|----|----|----|--|--|--|--|--|--|--|--|--|--|--|--|--|--|--|--|--|--|--|--|
| 1 | 2 | 3 | 4 | 5 | 6 | 7 | 8 | 9 | 10 | 11 | 12 | 13 | 14 | 15 | 16 | 17 | 18 | 19 | 20 | 21 | 22 | 23 | 24 | 25 | 26 | 27 | 28 | 29 | 30 | 31 | 32 | 33 | 34 | 35 | 36 | 37 | 38 | 39 | 40 | 41 | 42 | 43 | 44 | 45 | 46 | 47 | 48 | 49 | 50 | 51 | 52 | 53 | 54 | 55 | 56 | 57 | 58 | 59 | 60 | | | | | | | | | | | | | | | | | | | | |
| TITLE | | | | | | | | | | | | | | | | | | | | | | | | | | | | | | | | | | | | | | | | | | | | | | | | | | | | | | | | | | | | | | | | | | | | | | | | | | | | | | | |
| | | | | | | | | | | | | | | | | | | | | | | | | | | | | | | | | | | | | | | | | | | | | | | | | | | | | | | | | | | | | | | | | | | | | | | | | | | | | | | | |

Load Sheet for Card 1

Card 2 requires the following information to be specified. The input is punched in (4I5) format.

| | | | | | | | | | | | | | | | | | | | |
|------|---|---|---|---|------|---|---|---|----|-------|----|----|----|----|--------|----|----|----|----|
| 1 | 2 | 3 | 4 | 5 | 6 | 7 | 8 | 9 | 10 | 11 | 12 | 13 | 14 | 15 | 16 | 17 | 18 | 19 | 20 |
| NXTL | | | | | NZTL | | | | | IMOOH | | | | | IPRINT | | | | |
| | | | | | | | | | | | | | | | | | | | |

Load Sheet for Card 2

cc 1-5 NXTL total number of the sections defining the ship hull, $3 < \text{NXTL} < 41$. This is also the maximum x-stations (NX) in boundary-layer calculations.

- cc 11-20 ZB dimensional \bar{z} -value of the cross section, in feet or meters.
- cc 21-30 UE nondimensional inviscid velocity component in \bar{x} -direction,
 \bar{u}_e/u_{ref} .
- cc 31-40 VE nondimensional inviscid velocity component in \bar{y} -direction,
 \bar{v}_e/u_{ref} .
- cc 41-50 WE nondimensional inviscid velocity component in \bar{z} -direction,
 \bar{w}_e/u_{ref} .

It should be noted that Card 3 and Card (Set) 4 have to be input for all cross sections (NXTL)

A-2 Input for the Boundary-Layer Program

Card 1 contains the title of the problem under consideration. The input is punched as 80-column alphanumeric field as shown below.

| | | | | | | | | | | | | | | | | | | | | | | | | | | | | | | | | | | | | | | | | | | | | | | | | | | | | | | | | | | | |
|-------|---|---|---|---|---|---|---|---|----|----|----|----|----|----|----|----|----|----|----|----|----|----|----|----|----|----|----|----|----|----|----|----|----|----|----|----|----|----|----|----|----|----|----|----|----|----|----|----|----|----|----|----|----|----|----|----|----|----|----|
| 1 | 2 | 3 | 4 | 5 | 6 | 7 | 8 | 9 | 10 | 11 | 12 | 13 | 14 | 15 | 16 | 17 | 18 | 19 | 20 | 21 | 22 | 23 | 24 | 25 | 26 | 27 | 28 | 29 | 30 | 31 | 32 | 33 | 34 | 35 | 36 | 37 | 38 | 39 | 40 | 41 | 42 | 43 | 44 | 45 | 46 | 47 | 48 | 49 | 50 | 51 | 52 | 53 | 54 | 55 | 56 | 57 | 58 | 59 | 60 |
| TITLE | | | | | | | | | | | | | | | | | | | | | | | | | | | | | | | | | | | | | | | | | | | | | | | | | | | | | | | | | | | |

Load Sheet for Card 1

Card 2 contains the following information to be specified. It is punched in (6I5) format.

| | | | | | | | | | | | | | | | | | | | | | | | | | | | | | |
|-----|---|---|-----|---|---|--------|---|---|-----|----|----|-------|----|----|--------|----|----|----|----|----|----|----|----|----|----|----|----|----|----|
| 1 | 2 | 3 | 4 | 5 | 6 | 7 | 8 | 9 | 10 | 11 | 12 | 13 | 14 | 15 | 16 | 17 | 18 | 19 | 20 | 21 | 22 | 23 | 24 | 25 | 26 | 27 | 28 | 29 | 30 |
| NXT | | | NZT | | | NXSTRT | | | NTR | | | NSWCH | | | JPRINT | | | | | | | | | | | | | | |

Load Sheet for Card 2.

- cc 1-5 NXT the number of the last x-station (NX) to be calculated,
 $3 < \text{NXT} \leq \text{NXTL}$
- cc 6-10 NZT the number of the last z-station (NZ) to be calculated,
 $3 < \text{NZT} \leq \text{NZTL}$
- cc 11-15 NXSTRT the number of x-station (NX), referred to the geometry data, where boundary-layer calculations begin.
- cc 16-20 NTR the number of x-station (NX) where turbulent flow calculations begin. For laminar flow only, set $\text{NTR} > \text{NXT}$; for turbulent flow only, set $\text{NTR} = 1$. NTR will be overridden if laminar separation occurs.

- cc 21-25 NSWCH the number of x-station (NX) counted from NXSTRT where switching to "zigzag" scheme is made. If no switch is desired, set NSWCH > NXT. If NTR = 1, NSWCH may be arbitrary depending on the transverse pressure gradient; if NTR ≠ 1, NSWCH ≥ 3 is recommended.
- cc 26-30 JPRINT point interval by which the profiles are printed out. If JPRINT = 1, the velocity profiles are completely printed out from the wall to the boundary-layer edge.

Card 3 contains the following information to be specified. The input is in (5F10.0) format.

| | | | | | | | | | | | | | | | | | | | | | | | | | | | | | | | | | | | | | | | | | | | | | | | | | |
|------|---|---|---|---|---|---|---|---|----|-----|----|----|----|----|----|----|----|----|----|---------|----|----|----|----|----|----|----|----|----|-----|----|----|----|----|----|----|----|----|----|------|----|----|----|----|----|----|----|----|----|
| 1 | 2 | 3 | 4 | 5 | 6 | 7 | 8 | 9 | 10 | 11 | 12 | 13 | 14 | 15 | 16 | 17 | 18 | 19 | 20 | 21 | 22 | 23 | 24 | 25 | 26 | 27 | 28 | 29 | 30 | 31 | 32 | 33 | 34 | 35 | 36 | 37 | 38 | 39 | 40 | 41 | 42 | 43 | 44 | 45 | 46 | 47 | 48 | 49 | 50 |
| ETAE | | | | | | | | | | VGP | | | | | | | | | | DETA(1) | | | | | | | | | | CNU | | | | | | | | | | UREF | | | | | | | | | |

Load Sheet for Card 3

- cc 1-10 ETAE transformed boundary-layer thickness, η_{∞} for the first station. A value of 8 is usually sufficient. For NX > 1, it is computed internally.
- cc 11-20 VGP variable grid parameter, $K \geq 1.0$. For laminar flow, $K = 1.0$ is sufficient. For turbulent flow, it is a function of the Reynolds number, R_{∞} .
- cc 21-30 DETA(1) initial $\Delta\eta_1$ spacing at the wall. For laminar flow only, $\Delta\eta_1 = 0.2$ is suggested. For turbulent flow, it is also a function of R_{∞} . The suggested K and $\Delta\eta_1$ values for different Reynolds number are provided below.
- | | | | | |
|----------------|--------|--------|--------|--------|
| R_{∞} | 10^6 | 10^7 | 10^8 | 10^9 |
| K | 1.10 | 1.15 | 1.20 | 1.25 |
| $\Delta\eta_1$ | 0.015 | 0.01 | 0.0075 | 0.0050 |
- cc 31-40 CNU kinematic viscosity of the fluid, ν , in ft²/sec or m²/sec
- cc 41-50 UREF reference velocity, u_{ref} , in ft/sec or m/sec.

A-3 Output for the Geometry Program

The output of the geometry program includes the printout of the input data, the computed geometrical parameters, and the inviscid velocity components along the boundary-layer coordinate lines. The latter are also stored in external store unit (called TAPEDT) and serve as a part of the input data to

the boundary-layer program. The notation used in printing out the input data is the same as that used in the input. Therefore, only the meaning of the calculated geometrical parameters is interpreted here.

| | |
|-------|---|
| NX | station number of the x-station |
| x | x-value at NX station |
| z | normalized transverse coordinates in nonorthogonal boundary-layer coordinate system, measured from the keel ($z = 0.1$) to the free surface ($z = 1.0$) |
| YB | input or interpreted \bar{y} -value on the ship hull |
| ZB | input or interpreted \bar{z} -value on the ship hull |
| H1 | metric coefficient h_1 associated with the coordinate x |
| H2 | metric coefficient h_2 associated with the coordinate z |
| K1 | geodesic curvature, K_1 , of the x-coordinate line |
| K2 | geodesic curvature, K_2 , of the z-coordinate line |
| S1 | the physical surface distance S_1 measured along the x-coordinate line from the first x-station |
| K12 | geometric parameter, K_{12} |
| K21 | geometric parameter, K_{21} |
| THETA | angle, θ , between the coordinate lines in radian |
| UE | longitudinal velocity component, u_e , in the boundary-layer coordinates |
| WE | transverse velocity component, w_e , in the boundary-layer coordinates |
| C_p | pressure coefficient, $2(p - p_\infty)/\rho u_\infty^2$ |
| GIRTH | normalized surface distance along z-coordinate line, measured from the keel to the free surface. |

A-4 Output for the Boundary-Layer Program

The output of the program includes printout of the geometrical data passed from the geometry program on external storage unit 1, as well as tables of boundary-layer profiles and some important boundary-layer parameters. The notation for the geometrical data is the same as that in the geometry

program; therefore, only those associated with the boundary-layer parameters are given below.

1. The Profile Data

- J point number: profiles are printed from the wall outward. Not all points are printed and the interval is controlled through the input variable, JPRINT.
- ETA nondimensional boundary-layer variable η .
- Y normal distance from the wall, y , ft or m.
- U nondimensional velocity in x -direction in the boundary layer, $f' = u/u_e$.
- W nondimensional velocity in z -direction in the boundary layer, $g' = w/u_{ref}$.
- V derivative of U with respect to η , f'' .
- T derivative of W with respect to η , g'' .
- US velocity component in the boundary layer along the inviscid streamline direction, u_s .
- UN velocity component in the boundary layer normal to the inviscid streamline direction, u_n .
- USE total velocity at the edge of the boundary layer, u_{se} .
- BETA crossflow angle in degree, β , defined as
- $$\beta = \tan^{-1} u_n / u_s$$
- B nondimensional total eddy viscosity, $b = 1 + \epsilon/\nu$

2. Boundary-Layer Parameters

- CFS local skin-friction coefficient in the inviscid streamline direction, $c_{f_s} = 2\tau_{\omega_s} / \rho u_{se}^2$
- CFN local skin-friction coefficient normal to the inviscid streamline direction, $c_{f_n} = 2\tau_{\omega_n} / \rho u_{se}^2$
- DLSTS displacement thickness, δ^* , in feet or meters, defined as

$$\delta^* = \int_0^{\infty} (1 - u_s/u_{se}) dy$$

THTAS momentum thickness, θ_{11} , in feet or meters, defined as

$$\theta_{11} = \int_0^{\infty} u_s/u_{se} (1 - u_s/u_{se}) dy$$

HS shape factor, $H_{11} = \delta^*/\theta_{11}$

RTHTA Reynolds number based on momentum thickness, $R_{\theta} = \theta_{11} u_{se} / \nu$

CFX local skin-friction coefficient in \bar{x} -direction,

$$c_{f\bar{x}} = 2\tau_{\bar{x}} / \rho u_{ref}^2$$

REY Reynolds number, $R_x = u_{se} S_1 / \nu$

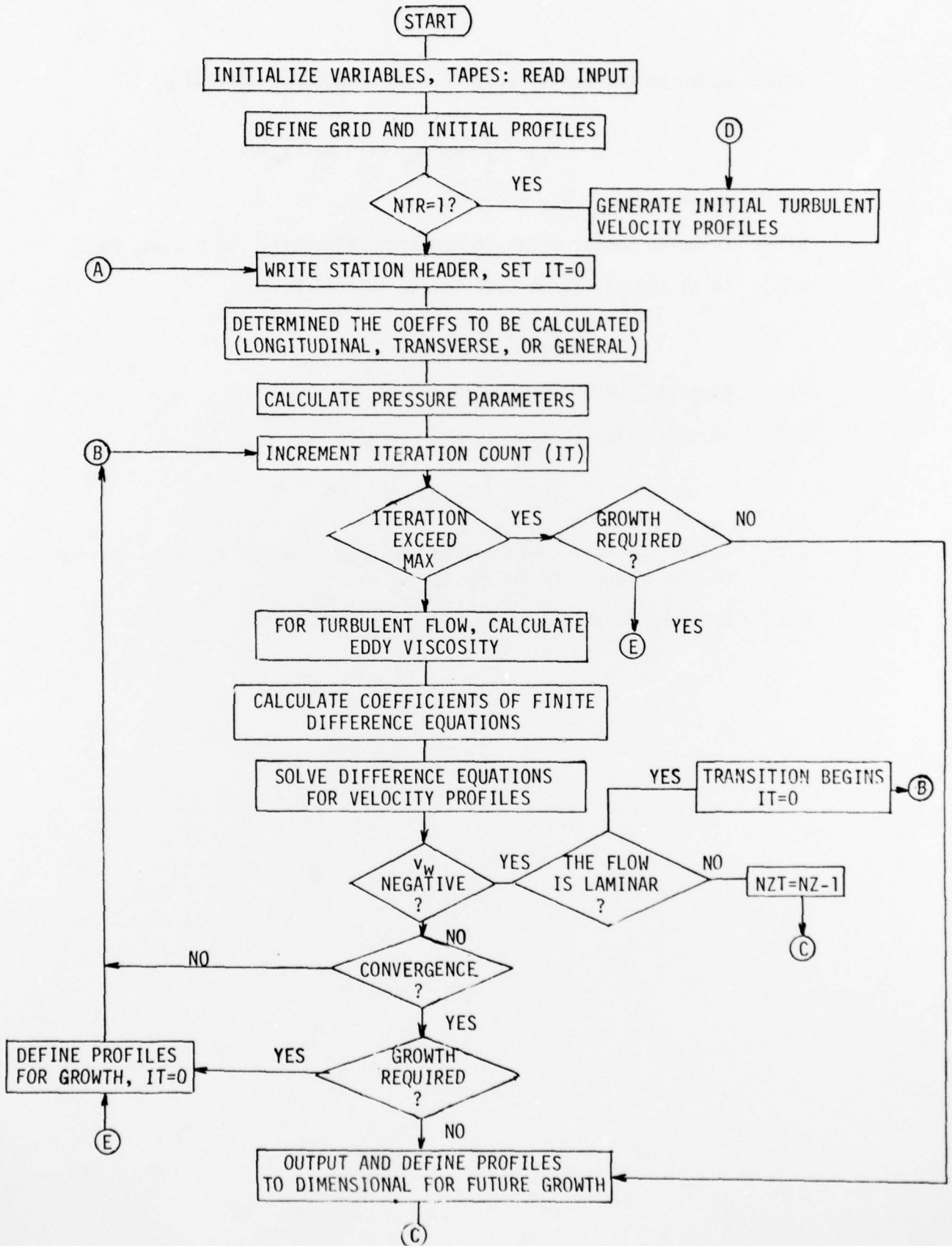
CFXB average skin-friction in \bar{x} -direction,

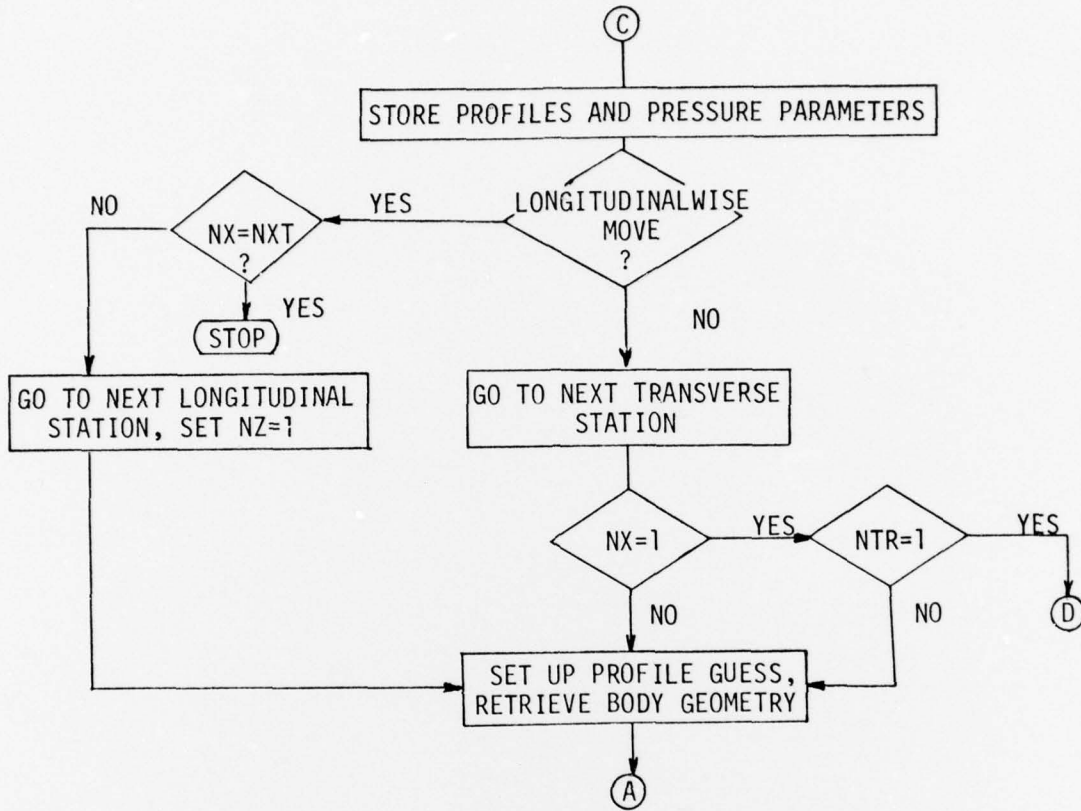
$$\bar{c}_{f\bar{x}} = \int_A c_{f\bar{x}} dA/A$$

AREA total ship hull surface area measured from the starting station to the current station

DELTA boundary-layer thickness, δ , in feet or meters

A-1. BASIC FLOW CHART FOR THE BOUNDARY-LAYER PROGRAM





Unclassified

SECURITY CLASSIFICATION OF THIS PAGE (When Data Entered)

| REPORT DOCUMENTATION PAGE | | READ INSTRUCTIONS BEFORE COMPLETING FORM |
|---|-----------------------|--|
| 1. REPORT NUMBER | 2. GOVT ACCESSION NO. | 3. RECIPIENT'S CATALOG NUMBER |
| 4. TITLE (and Subtitle) A General Method for Calculating Three-Dimensional Laminar and Turbulent Boundary Layers on Ship Hulls. | | 5. TYPE OF REPORT & PERIOD COVERED Final Technical Report July 1976 - October 1978 |
| 7. AUTHOR(s) Tuncer/Cebeci, K. C./Chang and Kalle/Kaups | | 6. PERFORMING ORG. REPORT NUMBER MDC-J7998 |
| 9. PERFORMING ORGANIZATION NAME AND ADDRESS McDonnell Douglas Corporation Douglas Aircraft Company 3855 Lakewood Blvd. Long Beach, Ca. 90846 | | 8. CONTRACT OR GRANT NUMBER(s) N00014-76-C-0950 |
| 11. CONTROLLING OFFICE NAME AND ADDRESS Naval Sea Systems Command David W. Taylor Naval Ship Research & Development Center Bethesda, Maryland 90084 | | 10. PROGRAM ELEMENT, PROJECT, TASK AREA & WORK UNIT NUMBERS SR 023 01 01 |
| 14. MONITORING AGENCY NAME & ADDRESS (if different from Controlling Office) <u>17 SR0230101</u> | | 12. REPORT DATE 11 October 1978 |
| | | 13. NUMBER OF PAGES 71 |
| | | 15. SECURITY CLASS. (of this report) Unclassified |
| | | 15a. DECLASSIFICATION/DOWNGRADING SCHEDULE |
| 16. DISTRIBUTION STATEMENT (of this Report) Approved for public release; distribution unlimited. | | |
| 17. DISTRIBUTION STATEMENT (of the abstract entered in Block 20, if different from Report) | | |
| 18. SUPPLEMENTARY NOTES | | |
| 19. KEY WORDS (Continue on reverse side if necessary and identify by block number) Three-dimensional boundary layers Turbulent flow Ship-hull geometry Viscous-inviscid interactions | | |
| 20. ABSTRACT (Continue on reverse side if necessary and identify by block number) A general method for representing the flow properties in the three-dimensional boundary layers around ship hulls of arbitrary shape is described. It makes use of an efficient two-point finite-difference scheme to solve the boundary-layer equations and includes an algebraic eddy-viscosity representation of the Reynolds-stress tensor. The numerical method contains novel and desirable features and allows the calculation of flows in which the circumferential velocity component contains regions of flow reversal across the boundary layer. | | |

DD FORM 1 JAN 73 1473

EDITION OF 1 NOV 65 IS OBSOLETE
S/N 0102-014-6601

Unclassified

SECURITY CLASSIFICATION OF THIS PAGE (When Data Entered)

63

116400

(over)
B

Unclassified

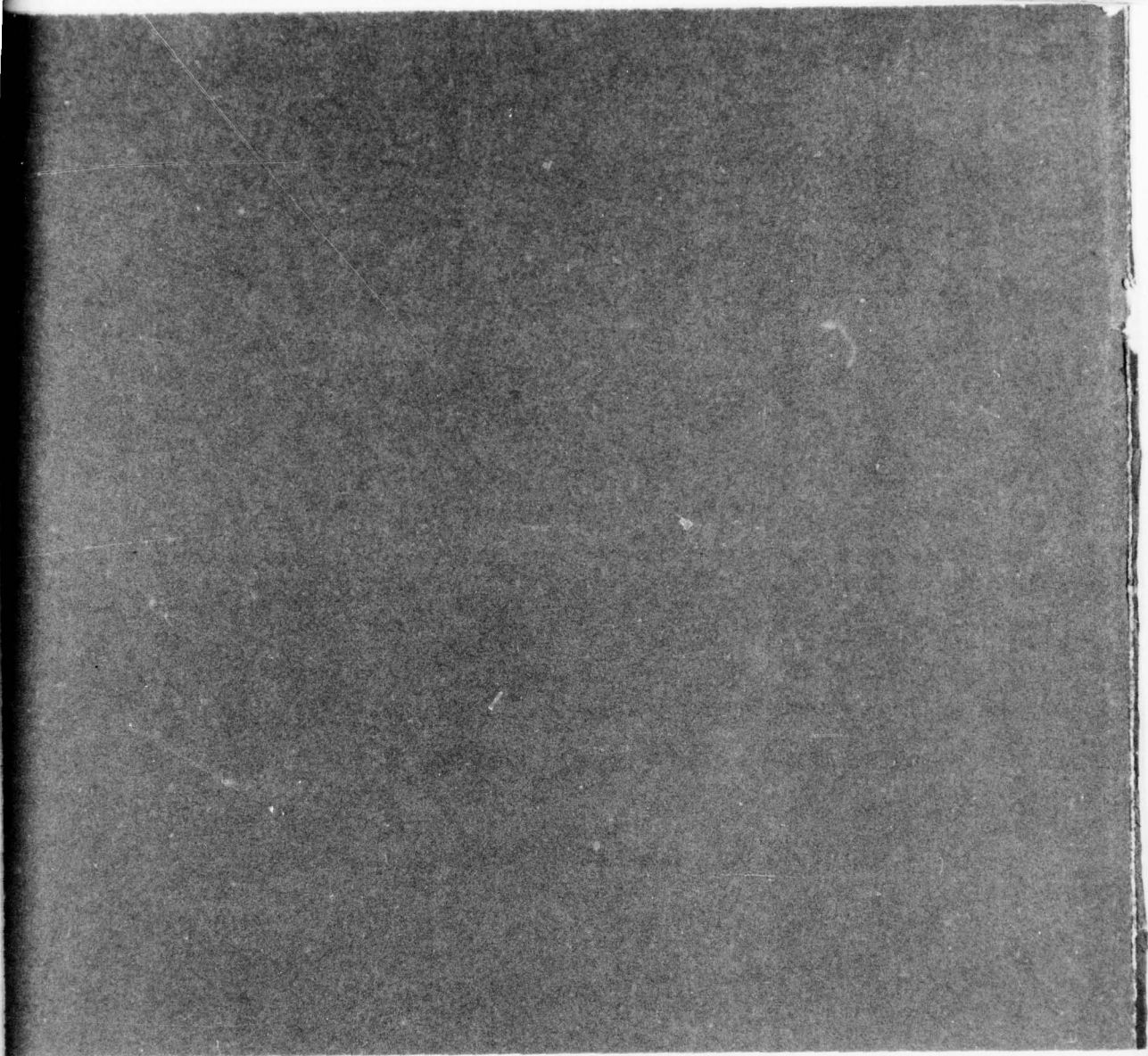
← SECURITY CLASSIFICATION OF THIS PAGE (When Data Entered)

The inviscid pressure distribution is determined with the Douglas-Neumann method which, if necessary, can conveniently allow for the boundary-layer displacement surface. To allow its application to ships, and particularly to those with double-elliptic and flat-bottomed hulls, a nonorthogonal coordinate system has been developed and is shown to be economical, precise and comparatively easy to use. Present calculations relate to zero Froude number but they can be extended to include the effects of a water wave and local regions of flow separation which may stem from bulbous-bow geometries.

△

Unclassified

SECURITY CLASSIFICATION OF THIS PAGE (When Data Entered)



DOUGLAS AIRCRAFT COMPANY

3855 Lakewood Boulevard, Long Beach, California 90846 (213) 593-5511

